

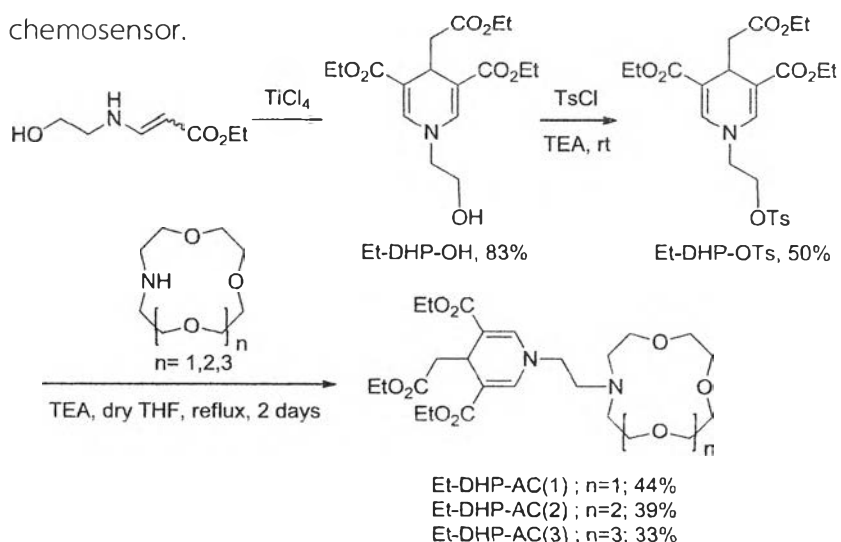
## CHAPTER III

### RESULTS AND DISCUSSION

#### 3.1 Synthesis and characterization of 1,4-dihydropyridine azacrown ether

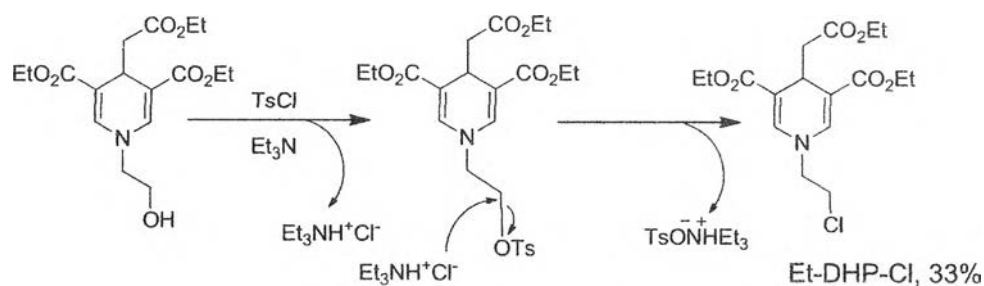
##### (Et-DHP-AC(1-3)).

Our fluorescence sensors were designed to possess DHP moiety as fluorophore and azacrown ether ring as water soluble and metal ion receiving unit. The synthesis of Et-DHP-OH started with the reaction of ethyl propiolate and ethanolamine in  $\text{CH}_2\text{Cl}_2$  at room temperature. Then the reaction mixture was completed overnight in the presence of  $\text{TiCl}_4$  Lewis acid to gain the corresponding  $\beta$ -amino acrylate in excellent yield (83%) based on our recently reported cyclotrimerization method [12]. The Et-DHP-OH was readily tosylated by using 4-toluenesulfonyl chloride (TsCl) and triethylamine (TEA) in  $\text{CH}_2\text{Cl}_2$  followed by the substitution with the azacrown ether ( $n=1-3$ ) to gain the corresponding Et-DHP-AC(1-3) in 44%, 39%, and 33% yields, respectively (**Scheme 3.1**). The structure of Et-DHP-AC(1-3) were confirmed by  $^1\text{H}$  NMR,  $^{13}\text{C}$  NMR, IR, and MALDI-TOF-MS, high resolution mass spectrometry (HRMS). In addition, DHP derivatives are readily soluble in aqueous media giving blue fluorescence which were found to be useful as a fluorescence chemosensor.



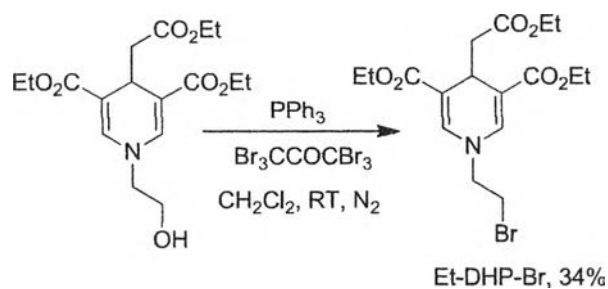
**Scheme 3.1** Synthesis of 1,4-dihydropyridine azacrown ether (Et-DHP-AC(1-3)).

The reasons for medium yielding (50%) in tosylation step from Et-DHP-OH to Et-DHP-OTs because there was a formation of by product (Et-DHP-Cl isolated yield 33 %). TsCl provides chloride ion that presumably attacks Et-DHP-OTs through nucleophilic substitution ( $S_N2$ ) reaction (**Scheme 3.2**). According to the literature reported by Ding and Kim [31, 32] for the sulfonation of R-OH, using sulfonyl chlorides such as metanesulfonyl chloride (MsCl) or *p*-toluenesulfonyl chloride (TsCl) with organic bases (DBU or TEA) occurred to give also chlorinated by product (R-Cl). Moreover, another reason for this medium yield of DHP-OTs was the use of silica gel for purification of crude Et-DHP-OTs. The silica gel acts as acidic phase that decomposes the sulfonyl group by elimination (E2) and so on. In case of Me-DHP-OTs, the product yield (20%) was lower than that of Et-DHP-OTs, because apart from two in reasons mentioned in the case of Et-DHP-OTs, its structure also has higher polarity compared to Et-DHP-OTs making it hard to purify by column chromatography.

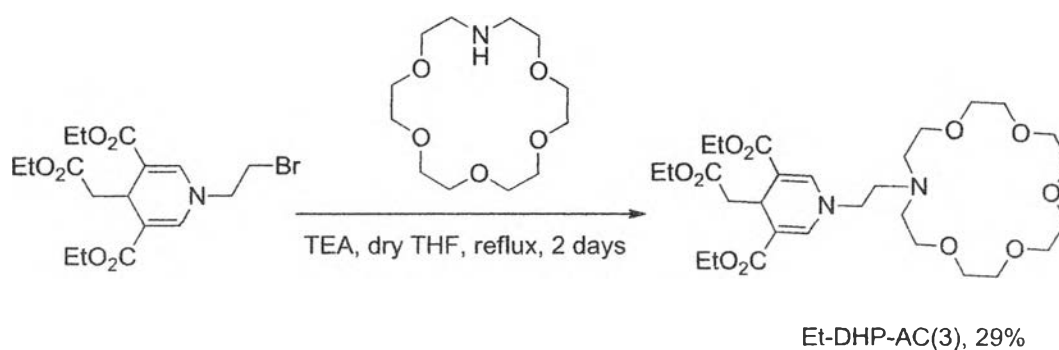


**Scheme 3.2** Possible reaction pathway.

Since there was a low yielding problem for the synthesis of Et-DHP-OTs, we therefore attempted to do the bromination of alcoholic compound in order to change the leaving group from OTs to Br by the bromination reaction using hexabromoacetone as a brominating agent [33] (**Scheme 3.3**). Even though, leaving group ability of Br is not as good as OTs, it is not that difference. So, as the results of percent yield between Et-DHP-OTs and Et-DHP-Br, there is no significant difference. The reason of low yielding of Et-DHP-Br is similar to the one previously mentioned in case of Et-DHP-OTs.



**Scheme 3.3** Bromination of Et-DHP-OH.



**Scheme 3.4** Substitution of Et-DHP-OH with azacrown ether.

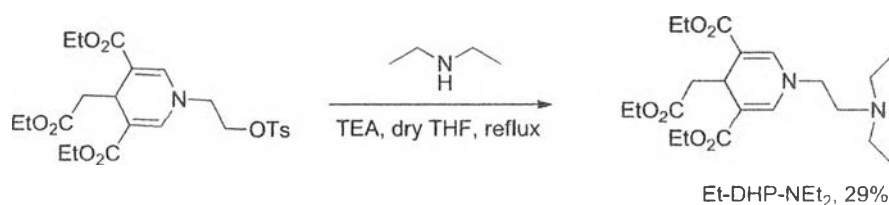
In conclusion, we have chosen the tosylation for the preparation of the substrate because the DHP-OTs could be obtained in higher %yield than the case of DHP-Br and hexabromoacetone ( $\text{Br}_3\text{CCOCBr}_3$ ) reagent is also rather expensive.

As the substitution with azacrown ether, this step gained target molecule in low %yield. There are 3 reasons to explain the possible reducing yield of target molecule. Firstly, once the azacrown ether with high polarity attached to DHP, it prefers to adhere to silica gel. The larger size of azacrown ether ( $n=1-3$ ) becomes, the more adhesiveness to the silica gel and hence the product will be less. Secondly, the azacrown ether may be protonated and dehydrated during quenching with cold water as well as the loss of product that the azacrown ether makes product rather dissolve in aqueous phase than in organic phase. For the solution on the matter, crude product of Et-DHP-OTs needs not to be quenched but should be evaporated instead to eliminate solvent and TEA residue before loading column chromatography. Finally, the leaving of azacrown ether can also be happened from the protonation by protons of silica gel during separation with column

chromatography. We suggest that the purification by silica gel column chromatography has to be basified prior to use and only used ethanol due to preventing it from the transesterification of triester within Et-DHP-AC.

### 3.2 Synthesis of 1,4-dihydropyridine diethylamine (Et-DHP-NEt<sub>2</sub>).

Et-DHP-NEt<sub>2</sub> was synthesized to be the reference compound in order to compare the different enhancement with Et-DHP-AC(1-3) in mixed solvent between acetonitrile and milliQ water (**Scheme 3.5**). Et-DHP-NEt<sub>2</sub> is low yielding because the possible protonation from NEt<sub>2</sub> liked DHP to NHet<sub>2</sub> as starting compound.



**Scheme 3.5** Substitution of Et-DHP-OH with diethylamine.

### 3.3 Characterization

#### 3.3.1 <sup>1</sup>H NMR of Et-DHP-OTs and Et-DHP-AC(1-3)

The <sup>1</sup>H NMR spectra of Et-DHP-OTs and Et-DHP-AC(1-3) in CDCl<sub>3</sub> are represented in **Figure 3.1**. All signals were assigned to all protons in each corresponding compound structure. As the evidence of the 1,4-DHP ring formation, the alkene peak at around 7 ppm (e) as singlet signal and around 4 ppm (d) as triplet respectively. As the starting substrate, Et-DHP-OTs possesses new doublet signal at 7.7 ppm (x) and 7.2 ppm (y) corresponding to its aromatic protons and new singlet signal at 2.37 ppm (z) corresponding to methyl group of toluene sulfonyl moiety. Et-DHP-AC(1-3) have each singlet signal at 7.14, 7.11, and 7.17 ppm, respectively. The methylene protons (-CH<sub>2</sub>-) linkage between DHP and azacrown ether were high field shifted from 4.12 to 2.70 and the methylene protons (-CH<sub>2</sub>-) of azacrown ether peaks are gathering together at 3.67-3.57 ppm as multiplet signal.

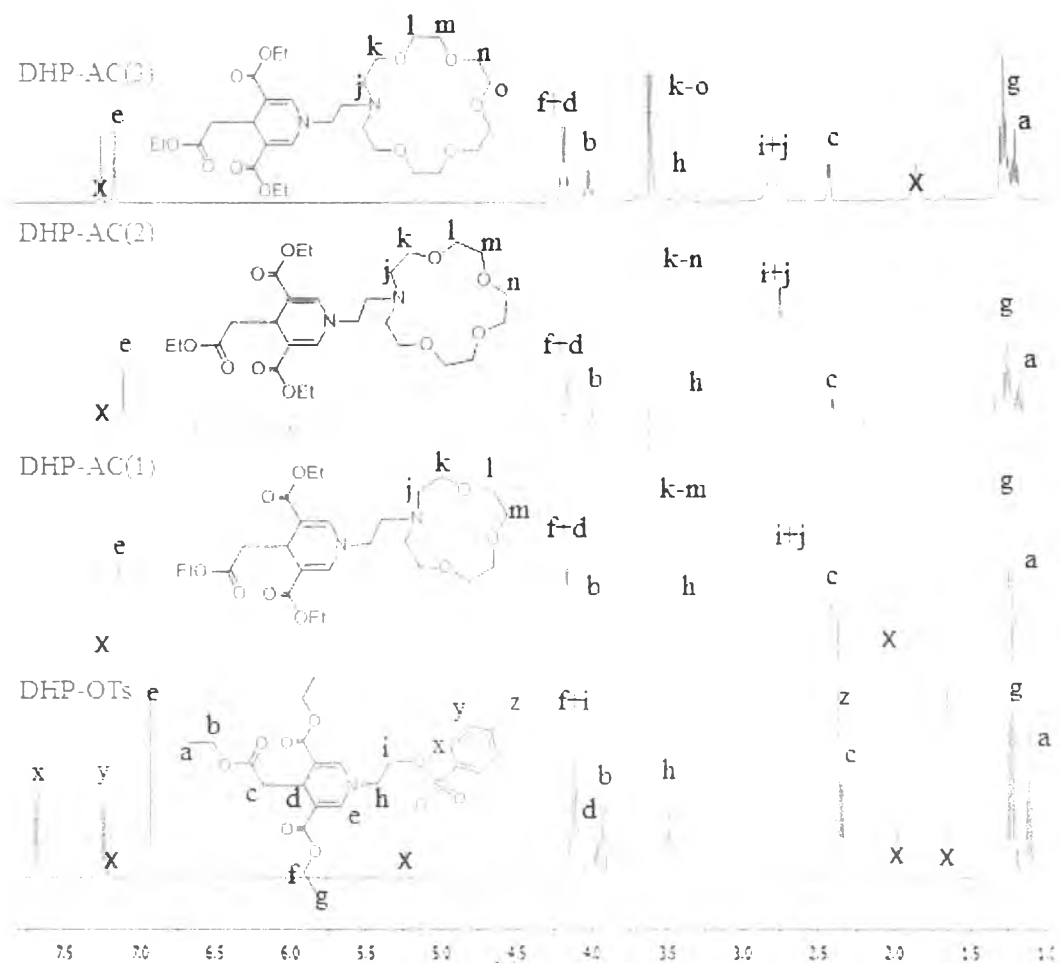


Figure 3.1  $^1\text{H}$  NMR (400) MHz of Et-DHP-OTs and Et-DHP-AC(1-3).

### 3.3.2 $^1\text{H}$ NMR of Et-DHP- $\text{NEt}_2$

The  $^1\text{H}$  NMR spectrum of Et-DHP- $\text{NEt}_2$  in  $\text{CDCl}_3$  is represented in Figure 3.2 compared with that of Et-DHP-OTs. As the doublet signal at 7.7 ppm (x) and 7.2 ppm (y) and singlet signal at 2.37 ppm (z) corresponding to toluene sulfonyl moiety. Et-DHP- $\text{NEt}_2$  demonstrated the methylene protons ( $-\text{CH}_2-$ ) linkage between DHP and diethylamine at 3.4 and 2.6 ppm. The other methylene protons ( $-\text{CH}_2-$ ) of diethylamine appear at 2.52 ppm as quartet signal, and the methyl protons ( $-\text{CH}_3$ ) of diethylamine appear at 1 ppm as triplet signal.

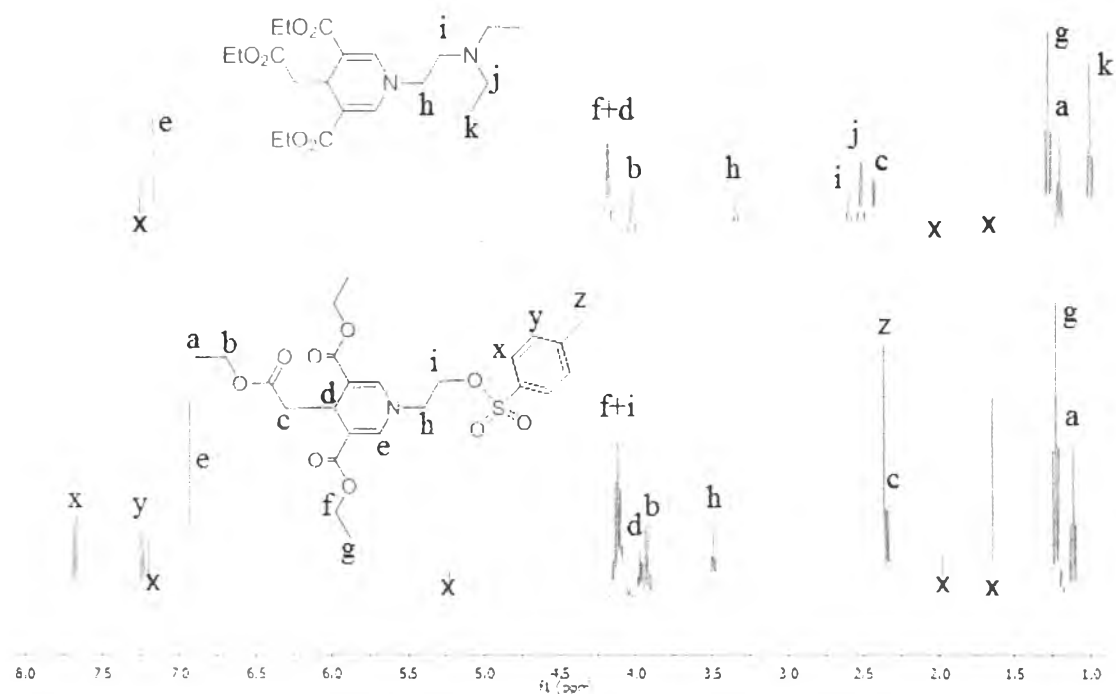
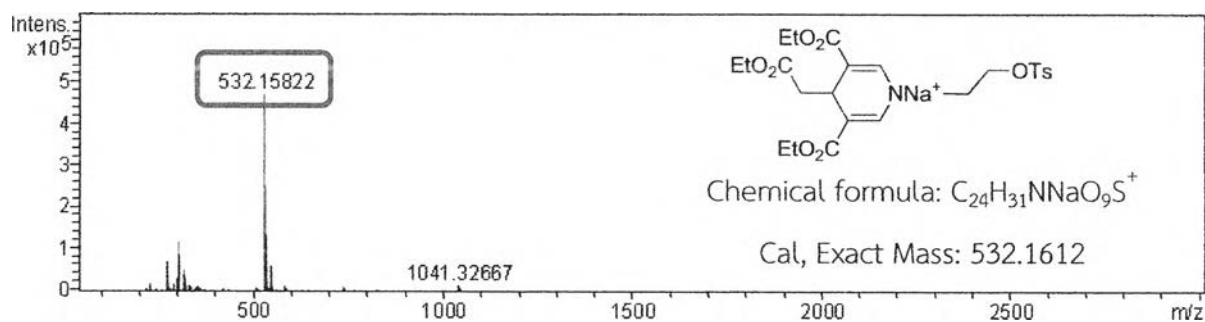


Figure 3.2  $^1\text{H}$  NMR (400) MHz of Et-DHP-OTs and Et-DHP-NEt<sub>2</sub>.

### 3.3.3 HRMS of Et-DHP-OTs, Et-DHP-AC(1-3), and Et-DHP-NEt<sub>2</sub>

The structural characterizations of the fluorophore were also confirmed by HRMS showing the molecular ion peaks corresponding or directly related to their molecular weights (Figure 3.3). HRMS was achieved only in the case of Et-DHP-OTs, Et-DHP-AC(1-3), and Et-DHP-NEt<sub>2</sub> for their novelties and complete characterizations.



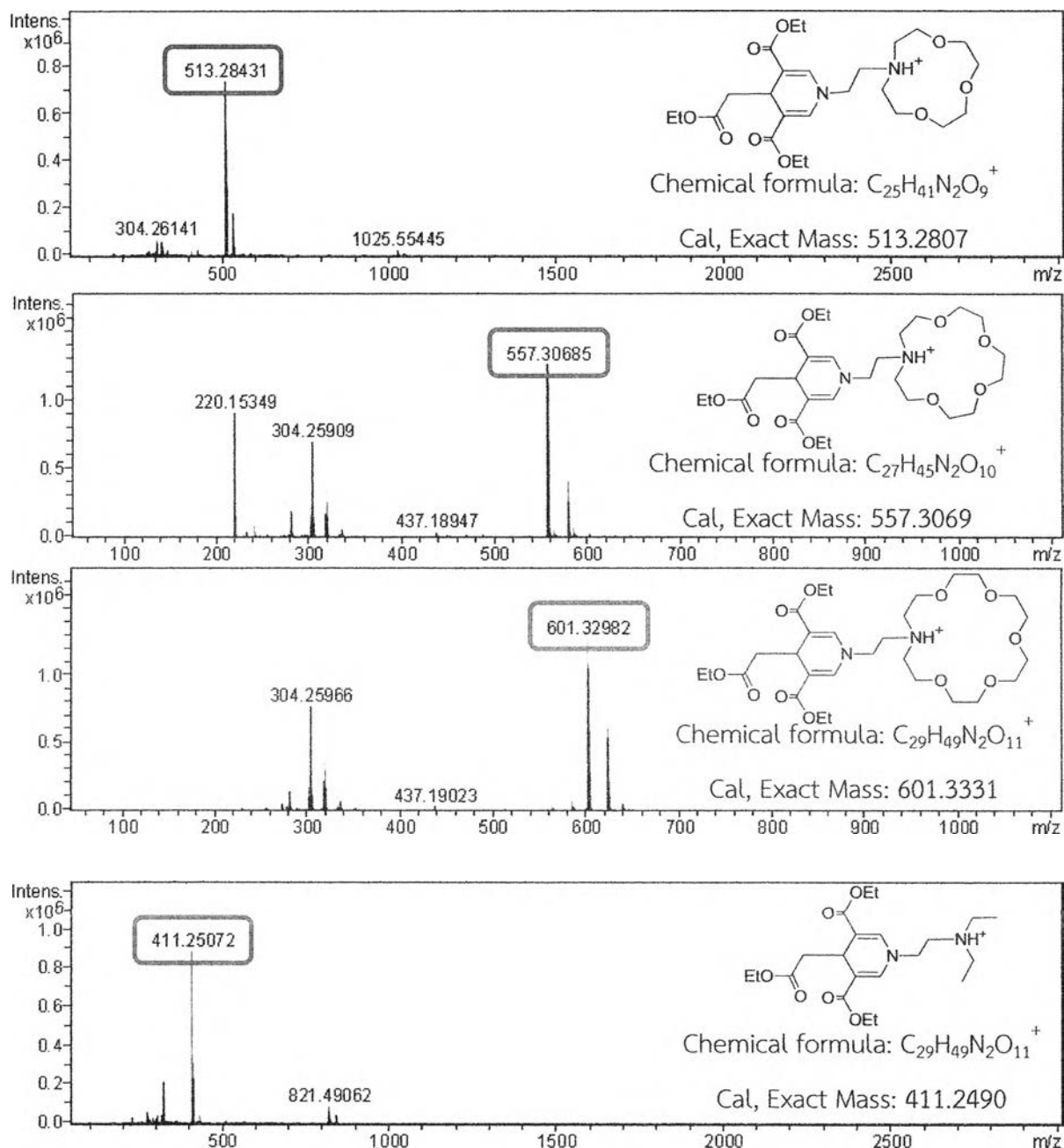


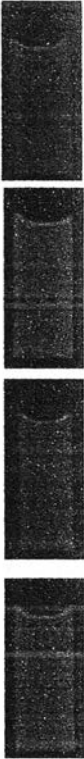
Figure 3.3 HRMS of Et-DHP-OTs, Et-DHP-AC(1-3), and Et-DHP-NEt<sub>2</sub>.

### 3.4 Photophysical property study

The photophysical property of Et-DHP-AC(1-3) and Et-DHP-NEt<sub>2</sub> at concentration 10  $\mu$ M in milliQ water was investigated by the spectrofluorometer and UV-Vis spectrophotometer. These compounds exhibited the wavelength of maximum absorbance ( $\lambda_{max}$ ) at 367, 369, 362, and 360 nm, respectively, with molar extinction

coefficients ( $\epsilon$ ) of  $3.7 \times 10^3$ ,  $6.9 \times 10^3$ ,  $5.8 \times 10^3$ , and  $6.6 \times 10^3 \text{ M}^{-1} \text{ cm}^{-1}$ , respectively. They showed characteristic  $\lambda_{\text{max}}$  of DHP moiety in the range of 360-370 nm. Also these compounds revealed the similar emission peak at around 439 nm with fluorescent quantum efficiencies ( $\Phi_f$ ) of 0.41, 0.45, 0.46, and 0.50, respectively (Table 3.1 and Figure 3.4).

Table 3.1 Photophysical property of Et-DHP-AC(1-3) and Et-DHP-NEt<sub>2</sub> in aqueous solution.

Compound	Absorption		Emission		Appearance under black light (10 $\mu$ M)
	$\lambda_{\text{max}}$ (nm)	$\epsilon$ ( $\text{M}^{-1} \text{ cm}^{-1}$ )	$\lambda_{\text{max}}$ nm	$\Phi_f^a$	
Et-DHP-AC(1)	367	$3.7 \times 10^3$	439	0.45	
Et-DHP-AC(2)	369	$6.9 \times 10^3$	439	0.41	
Et-DHP-AC(3)	362 368 <sup>b</sup>	$5.8 \times 10^3$ $5.8 \times 10^{3b}$	439 439 <sup>b</sup>	0.46 0.17 <sup>b</sup>	
Et-DHP-NEt <sub>2</sub>	360	$6.6 \times 10^3$	439	0.50	

<sup>a</sup>Quinine sulfate in 0.1 M H<sub>2</sub>SO<sub>4</sub> ( $\Phi_F = 0.54$ ) was used as the reference.

<sup>b</sup>Experiment of Et-DHP-AC(3) in acetonitrile and milliQ water (70:30 v/v).



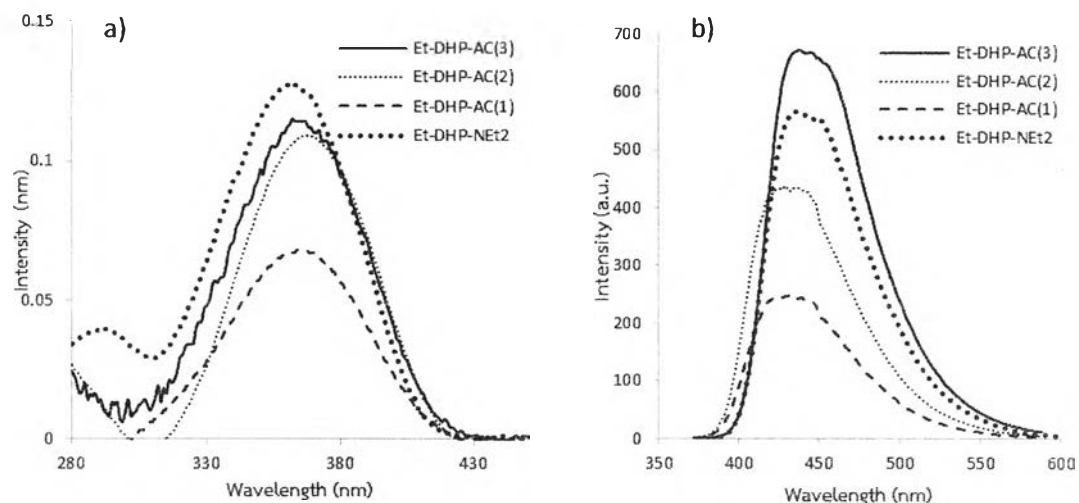


**Figure 3.4** a) Absorption spectra b) Fluorescence spectra of 10  $\mu\text{M}$  Et-DHP-AC(1-3) and Et-DHP-NEt<sub>2</sub> in milliQ water.

### 3.6 Metal ion sensor of Et-DHP-AC(3)

#### 3.6.1 Fluorescence emission of Et-DHP-AC(1-3) response against metal ions

Since Et-DHP-AC(3) has high extinction coefficient, quantum yield with blue emission appearance, it was therefore selected for further investigation in sensing applications. The fluorescence responses of Et-DHP-AC(3) (10  $\mu\text{M}$ ) in aqueous media towards 21 metal ions ( $\text{Na}^+$ ,  $\text{Ca}^{2+}$ ,  $\text{Sr}^{2+}$ ,  $\text{Ba}^{2+}$ ,  $\text{Al}^{3+}$ ,  $\text{Ag}^+$ ,  $\text{Bi}^{3+}$ ,  $\text{Cr}^{6+}$ ,  $\text{Hg}^{2+}$ ,  $\text{Pb}^{2+}$ ,  $\text{Fe}^{2+}$ ,  $\text{Fe}^{3+}$ ,  $\text{Co}^{2+}$ ,  $\text{Zn}^{2+}$ ,  $\text{Cd}^{2+}$ ,  $\text{Cu}^{2+}$ ,  $\text{K}^+$ ,  $\text{Li}^+$ ,  $\text{Mg}^{2+}$ ,  $\text{Mn}^{2+}$ ,  $\text{Ni}^{2+}$ ) were illustrated in the fluorescence (Figure 3.5 and Figure 3.6.). Fortunately, Et-DHP-AC(3) was selective and complete quenching at least reaction time with  $\text{Au}^{3+}$ .

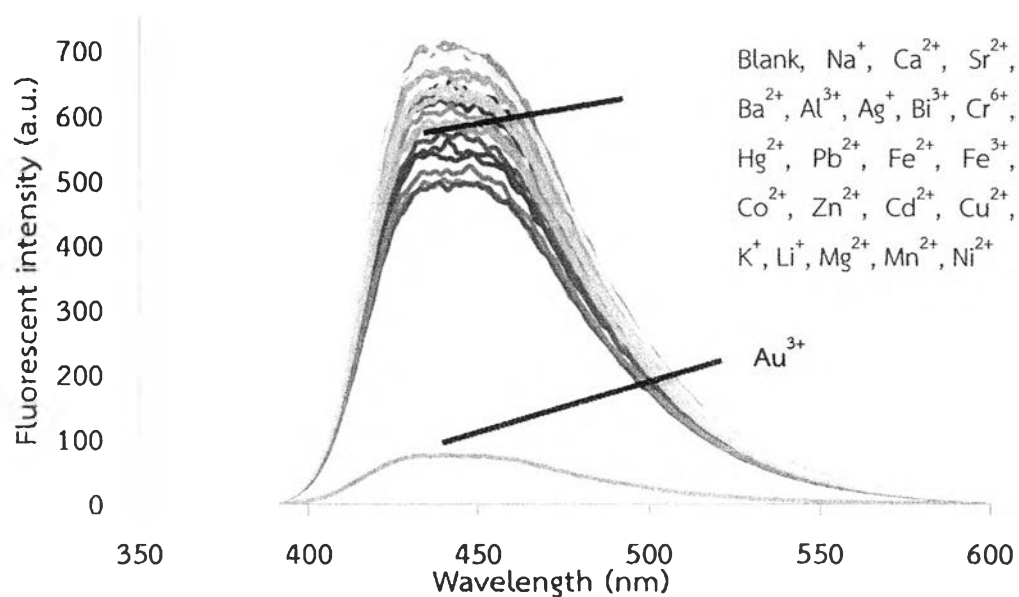


Figure 3.5 Fluorescence quenching profile of Et-DHP-AC(3) (10  $\mu\text{M}$ ), 10 minutes after addition of each metal ion (100  $\mu\text{M}$ ) in milliQ water ( $\lambda_{\text{ex}} = 362 \text{ nm}$ ).

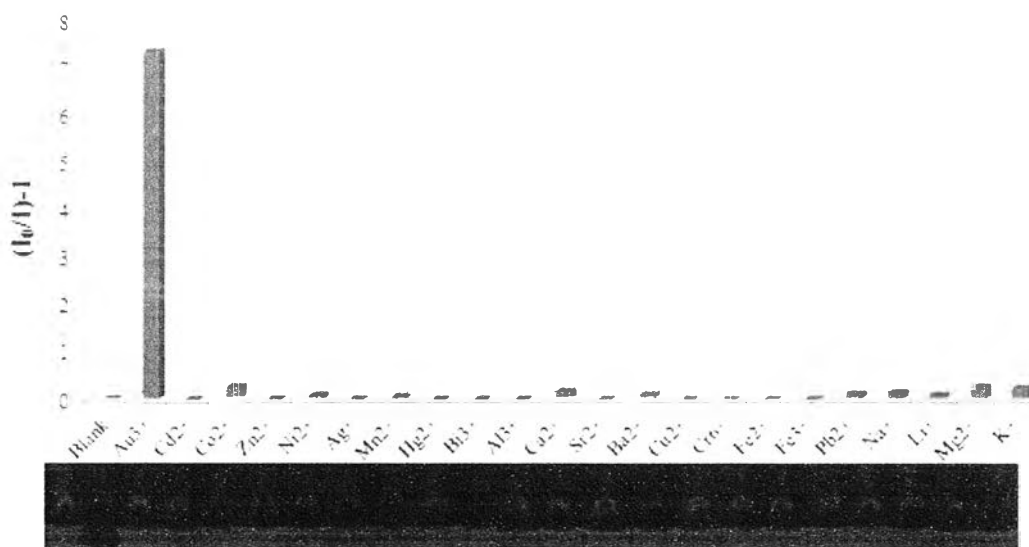
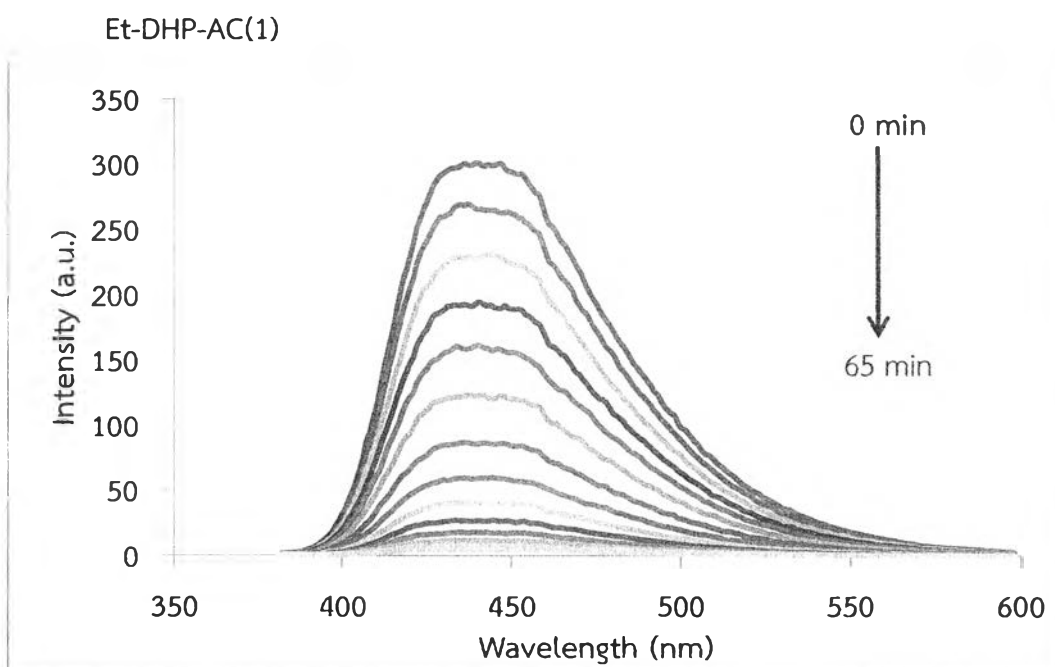


Figure 3.6 Fluorescence response  $(I_0/I)-1$  of Et-DHP-AC(3) (10  $\mu\text{M}$ ), 20 minutes after addition of each metal ion (100  $\mu\text{M}$ ) in milliQ water ( $\lambda_{\text{ex}} = 362 \text{ nm}$ ). The photo shows fluorescence appearance under black light of Et-DHP-AC(3) (10  $\mu\text{M}$ ) upon addition of metal ion (100  $\mu\text{M}$ ).

### 3.6.2 Reaction time with $\text{Au}^{3+}$ of Et-DHP-AC(1-3), Et-DHP-OH and Et-DHP- $\text{NEt}_2$

As Et-DHP-AC(3) was selectively quenched with  $\text{Au}^{3+}$  in aqueous solution. We then carried out the metal ion detection of other DHP derivatives (Et-DHP-AC(1-2), Et-DHP-OH, and Et-DHP- $\text{NEt}_2$ ). As the results, all sensors were proven to also selectively quench with  $\text{Au}^{3+}$ , but the reactions of them with  $\text{Au}^{3+}$  occurred in the different rates and completely quenched the fluorescent signal of DHP unit at 65, 55, 15, 35, and 55 minutes respectively. Et-DHP-AC(3) displayed the fastest complete quenching presumably since the influence of suitable size of aza-18-crown-6 induces  $\text{Au}^{3+}$  to reach the reactive site of DHP ring followed by the oxidation reaction.



**Figure 3.7** Fluorescence spectra of 10  $\mu\text{M}$  Et-DHP-AC(1) and 100  $\mu\text{M}$   $\text{Au}^{3+}$  in milliQ water.

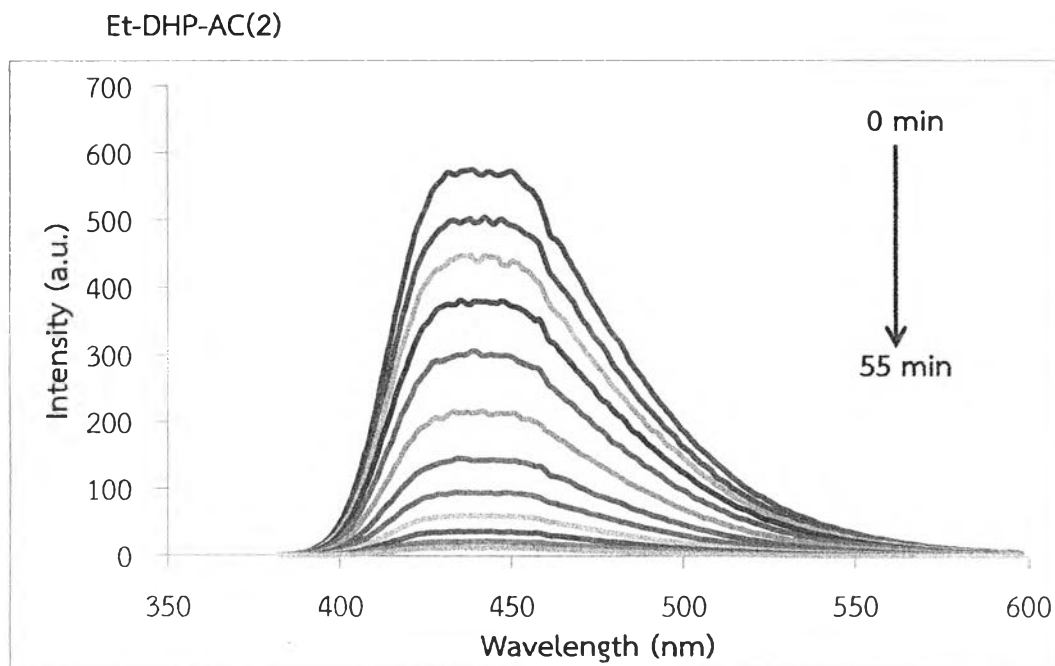


Figure 3.8 Fluorescence spectra of 10 μM Et-DHP-AC(2) and 100 μM Au<sup>3+</sup> in milliQ water.

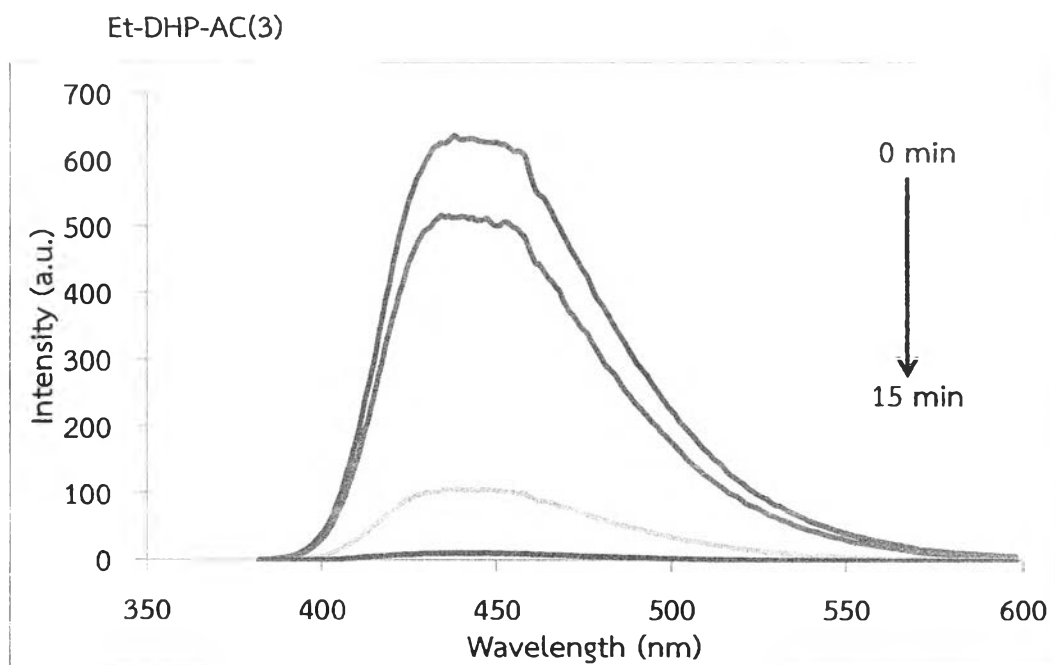


Figure 3.9 Fluorescence spectra of 10 μM Et-DHP-AC(3) and 100 μM Au<sup>3+</sup> in milliQ water.

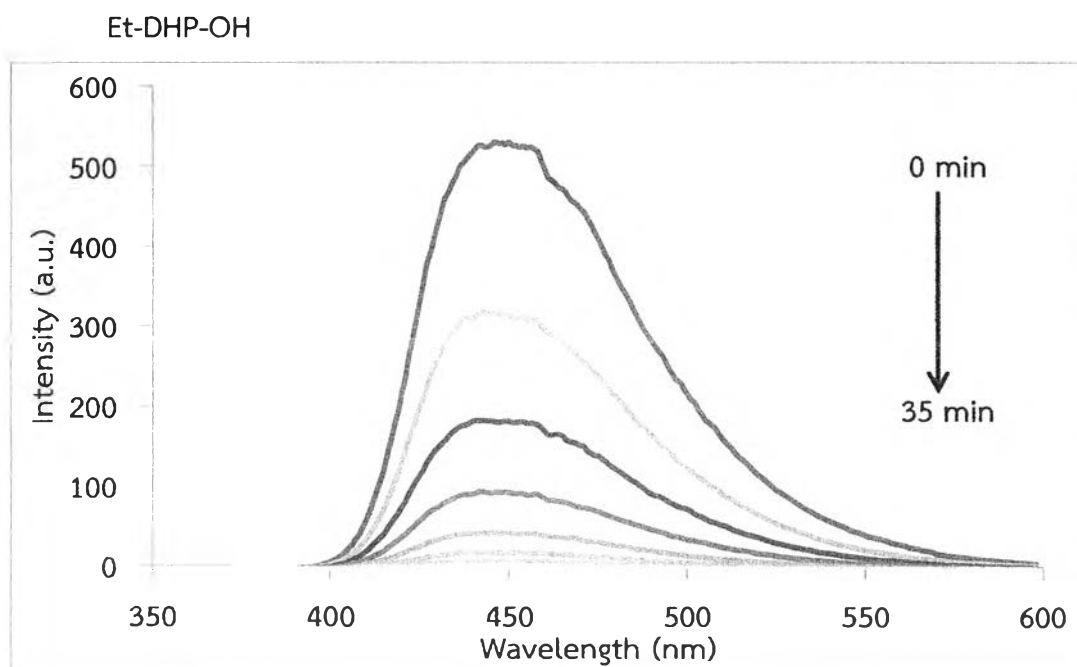


Figure 3.10 Fluorescence spectra of 10  $\mu\text{M}$  Et-DHP-OH and 100  $\mu\text{M}$  Au<sup>3+</sup> in milliQ water.

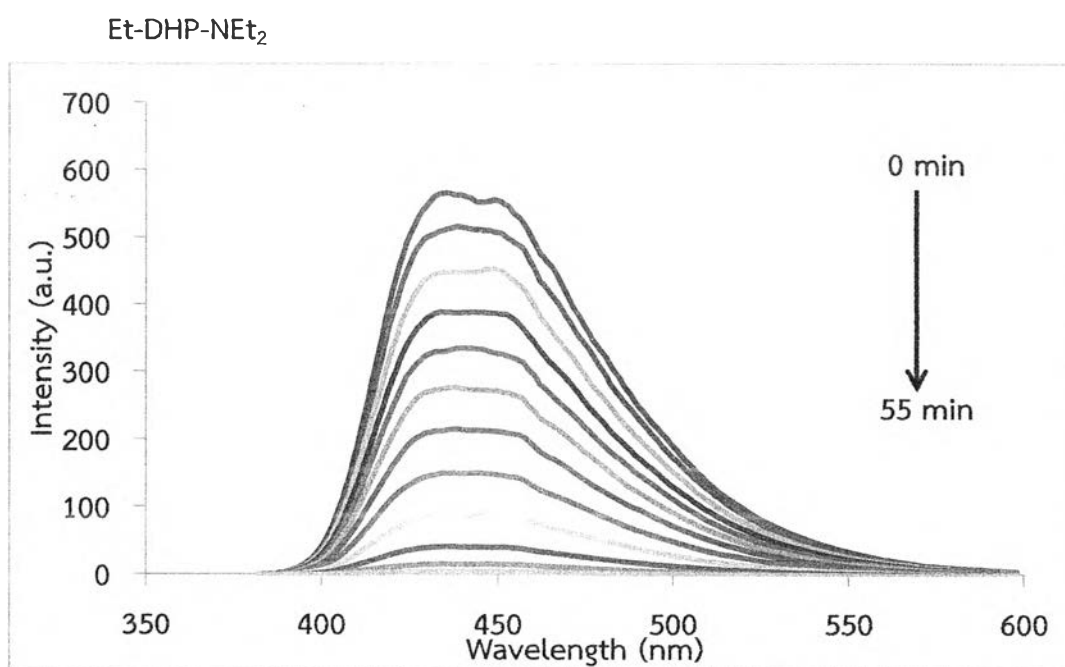
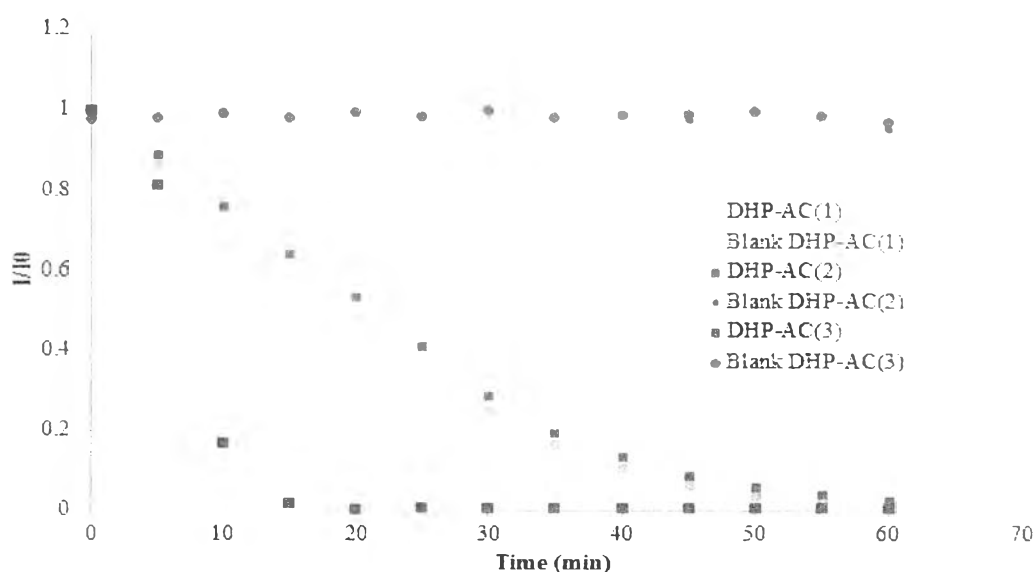


Figure 3.11 Fluorescence spectra of 10  $\mu\text{M}$  Et-DHP-NEt<sub>2</sub> and 100  $\mu\text{M}$  Au<sup>3+</sup> in milliQ water.

According to the results of the time dependent quenching of all DHP derivatives, Et-DHP-AC(3) demonstrated the fastest complete quenching profile. In order to compare the reaction times of DHP-AC(1-3) against  $\text{Au}^{3+}$ , the monitoring of fluorescence intensities of Et-DHP-AC(1-3) against  $\text{Au}^{3+}$  (10 equiv) was achieved in 60 minutes and summarized into **Figure 3.12** including the results of all blank DHP-AC(1-3) without  $\text{Au}^{3+}$ . The kinetic results exhibited that the intensity rapidly decreased and reached the minimum of fluorescence intensity after 20 minutes. Since the quenching process was relatively slow, we assumed that it was caused by chemical reaction rather than the fast dynamic or static quenching mechanism.



**Figure 3.12** Fluorescence quenching profile of Et-DHP-AC(1-3) (10  $\mu\text{M}$ ) 0 to 60 minutes after addition of  $\text{Au}^{3+}$  0 and 10 equiv in milliQ water ( $\lambda_{\text{ex}} = 362, 369,$  and  $367$  nm respectively).

### 3.6.3 UV-Vis spectral responses of Et-DHP-AC(3) to Au<sup>3+</sup>

In order to gain insightful information about the quenching mechanism, time tracking UV-Vis spectroscopy of Et-DHP-AC(3) with 10 equiv of Au<sup>3+</sup> was carried out from 1 minute to 30 minutes. As a result, the absorbance spectrum of Et-DHP-AC(3) was immediately altered from the beginning. The aromatic band at 286 nm rapidly appeared, while the DHP band at 362 nm gradually decreased confirming the possibility of structural change within the DHP ring (Figure 3.13). This hypsochromic shift is probably caused by the aromatization of the DHP ring to a pyridinium ring (290 nm).

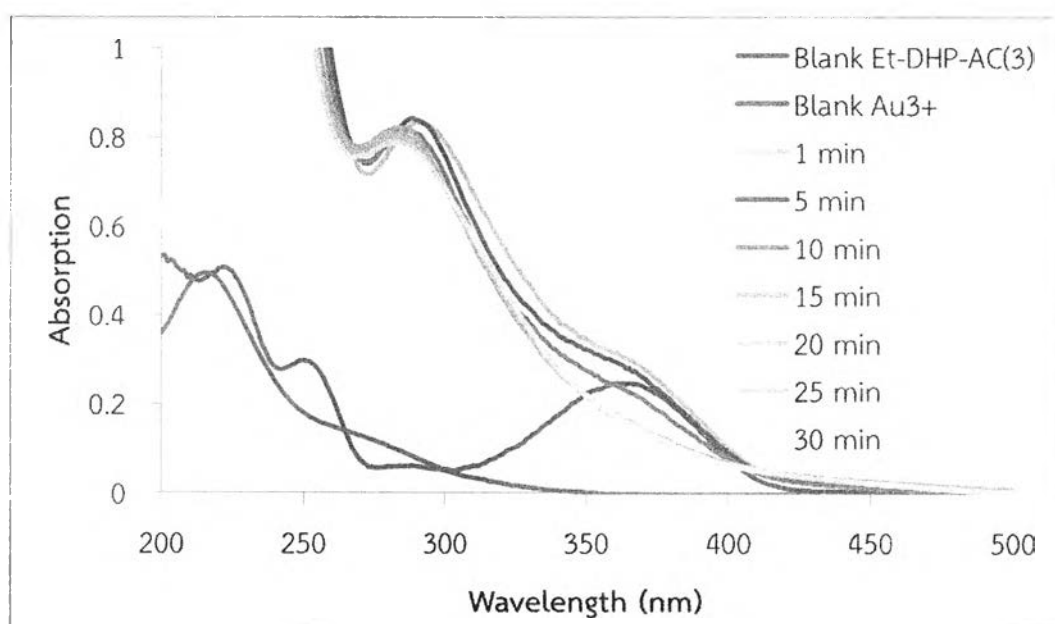
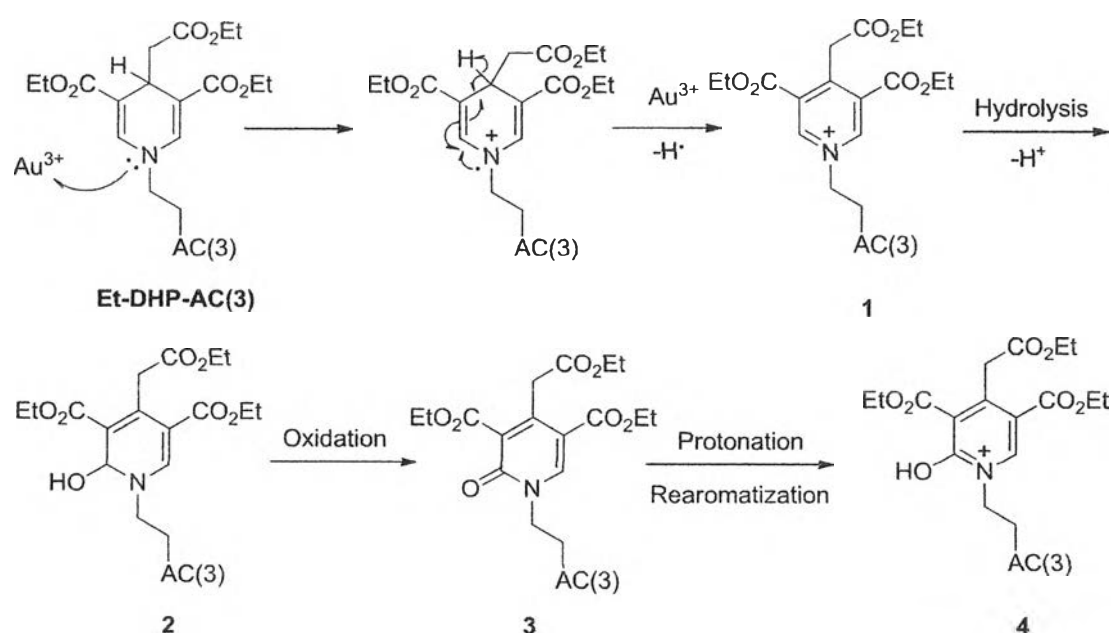


**Figure 3.13** UV-Vis spectra of Et-DHP-AC(1-3) (30  $\mu\text{M}$ ) 1 to 30 minutes after addition of Au<sup>3+</sup> (300  $\mu\text{M}$ ) in milliQ water.

### 3.6.4 $^1\text{H}$ NMR experiment

$^1\text{H}$  NMR experiment was conducted to seek more evidence to support this pyridine ring formation from the DHP ring. Due to the solubility limitation, only 1 equiv of  $\text{Au}^{3+}$  could be used. As a result, there was a significant change in the  $^1\text{H}$  NMR spectrum within 25 minutes; The signal of methylene protons ( $-\text{CH}_2-$ ) of azacrown ether were broad and low integration (**Figure 3.14**), concluding that azacrown ether assists the induction of  $\text{Au}^{3+}$  to approach the reactive site (DHP ring). Furthermore, the signals of two olefinic protons in DHP ring at 7.17 ppm decreased (**Figure 3.14**), referring to the partial loss of the DHP structure. We believe that the DHP ring was oxidized into a pyridinium ring by  $\text{Au}^{3+}$  (**Scheme 3.6**), since the MS spectrum of the product also showed strong signal at  $m/z = 598.858$  (**Figure 3.15**) in good agreement with the molecular weight of the proposed pyridinium product **1**. Nevertheless, it is not clear to us at this moment for the observation of two  $^1\text{H}$  NMR signals at 9-10 ppm for the two supposedly equivalent protons of pyridinium ring. After that, the changing from pyridinium to hydroxyl compound **2** by the hydrolysis and then oxidized to oxo compound **3** that was possibly protonated to hydroxyl pyridinium compound **4**. Many small peaks in range of 9-10 ppm appearing in the MS spectrum (**Figure 3.15**) may be mixture product of compounds (**1-4**). Unfortunately, our attempt to isolate the product for better defined characterization has not yet been successful due to the instability of product.



Scheme 3.6 Proposed mechanism for the formation of **1** and **2**.



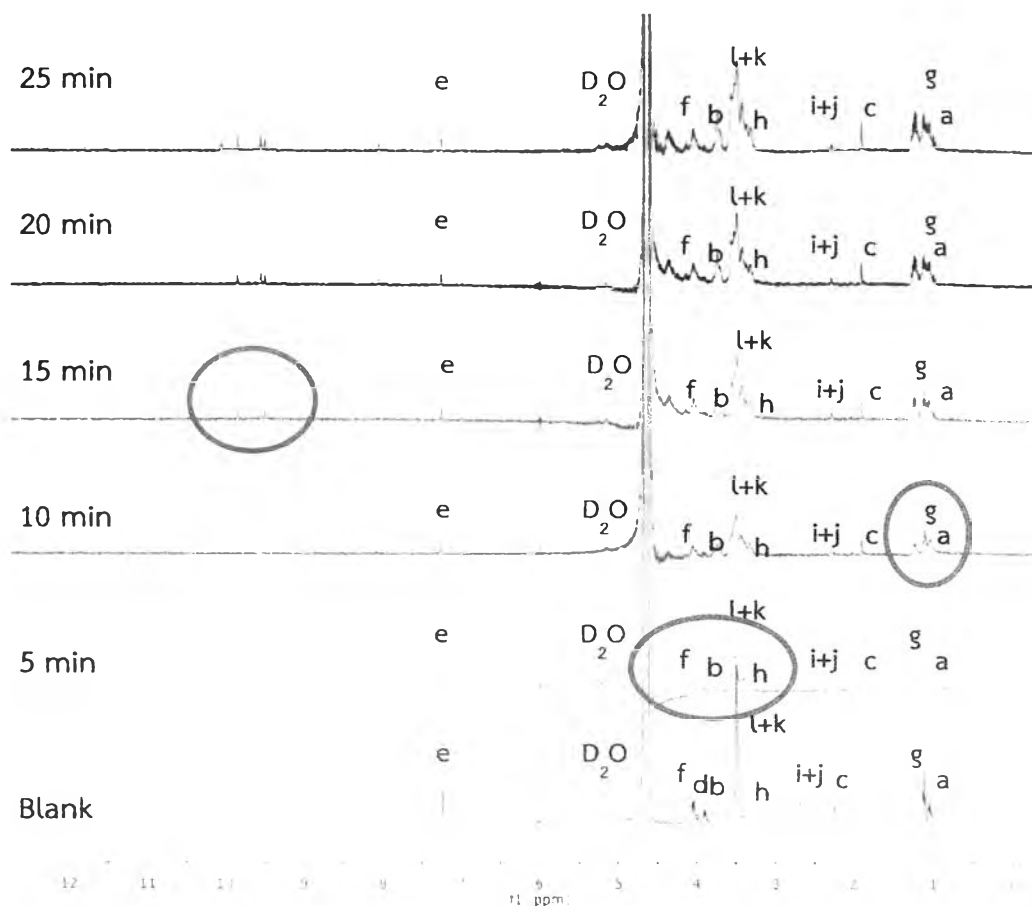


Figure 3.14  $^1\text{H}$  NMR spectra of Et-DHP-AC(3) in  $\text{D}_2\text{O}$ , 25 min adding of 1 equiv  $\text{Au}^{3+}$ .

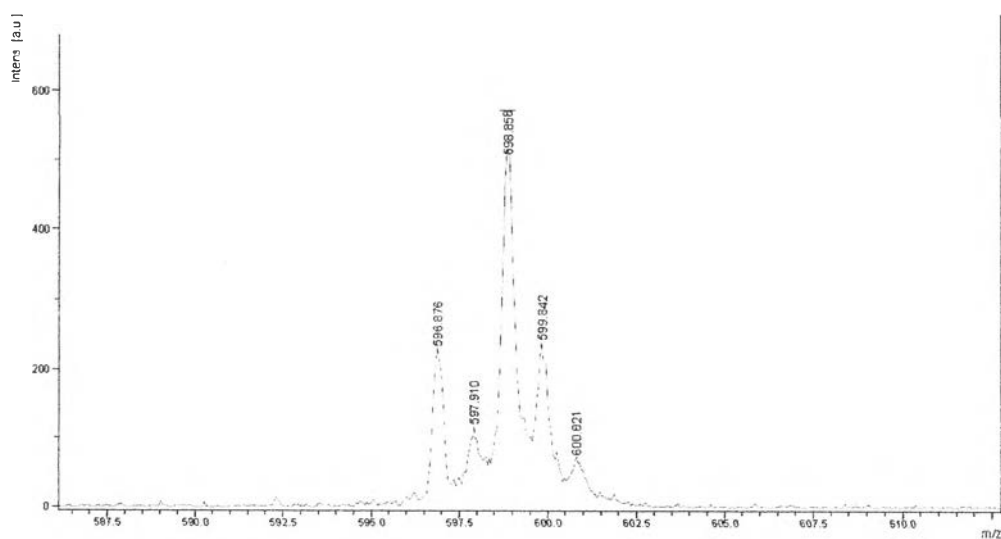
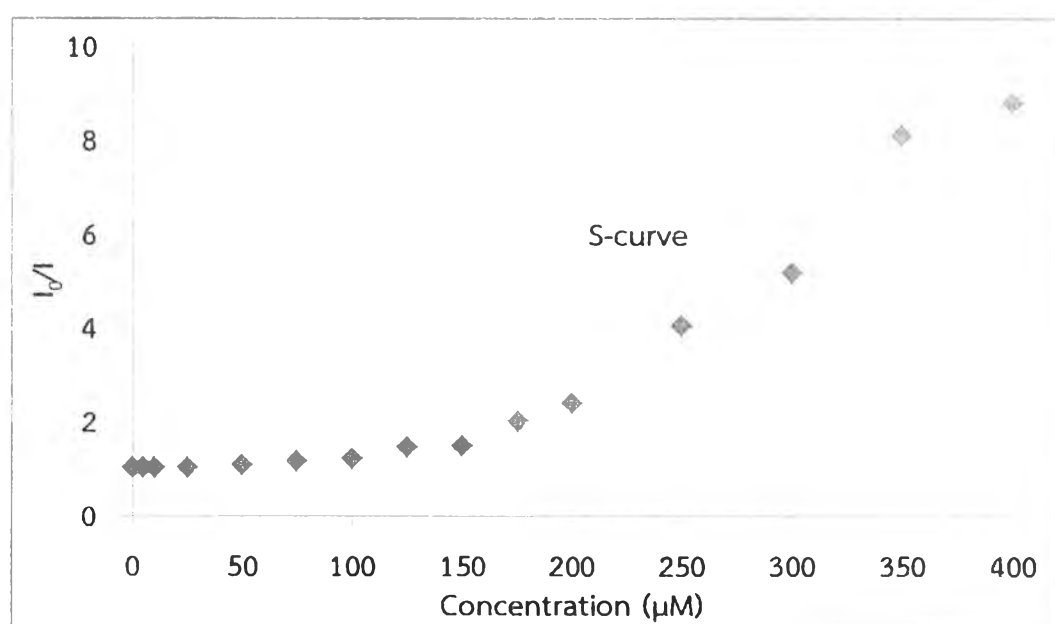


Figure 3.15 MALDI-TOF of pyridinium ring

### 3.6.5 Fluorescence titration of Et-DHP-AC(3) to Au<sup>3+</sup>

We have also carried out the fluorescence titration of Et-DHP-AC(3) (5  $\mu\text{M}$ ) to Au<sup>3+</sup> ion (5 to 400  $\mu\text{M}$ ) in aqueous solution for 10 minutes (**Figure 3.16**). As the concentration of Au<sup>3+</sup> ion increased, the quenching of Et-DHP-AC(3) started gradually and complete at 400  $\mu\text{M}$  (80 equiv) of Au<sup>3+</sup> ion. The results of the fluorescence titration showed that the concentration of gold ion has an effect on the reaction rate of the gold-induced fluorescence quenching of Et-DHP-AC(3), again possibly due to the structural change from DHP to pyridinium derivative. The results also confirmed that the quenching was not the complexation between Et-DHP-AC(3) and Au<sup>3+</sup> ion. The detection limit of Et-DHP-AC(3) cannot be calculated by using the Stern-Volmer plot because of the nonlinear curve (s-curve) (**Figure 3.17**).



**Figure 3.16** Fluorescence change of Et-DHP-AC(3) (5  $\mu\text{M}$ ) with the addition of Au<sup>3+</sup> (0 to 400  $\mu\text{M}$ ) in milliQ water at 10 minutes ( $\lambda_{\text{ex}} = 362 \text{ nm}$ ).

However, the lowest detectable concentration (LDC) of  $\text{Au}^{3+}$  was determined from initial rate of reaction. Bhalla V. et al [34] reported the method for calculating LDC from this equation:

$$\text{LDC} = C_F \times C_T$$

$C_F$  = concentration of fluorophore

$C_T$  = equiv concentration of titrant at which change observed

As a consequence, the LDC plotted graph between intensity and equiv concentration of gold ion was equal to 50  $\mu\text{M}$ .

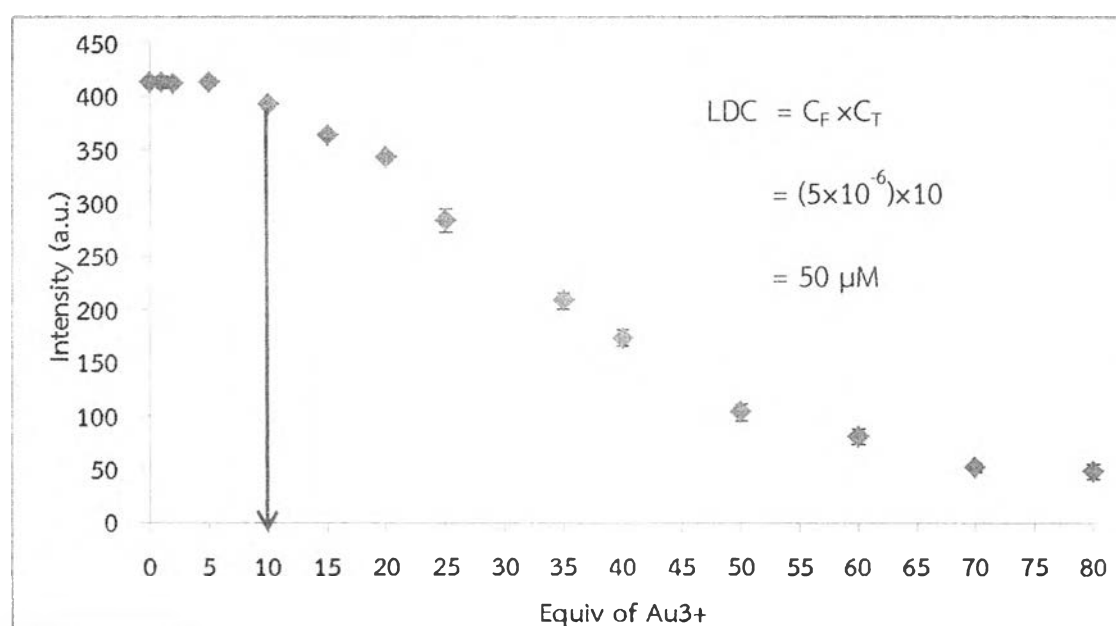


**Figure 3.17** Fluorescence change of Et-DHP-AC(3) (5  $\mu\text{M}$ ) with the addition of  $\text{Au}^{3+}$  (0 to 80 equiv) in milliQ water at 10 minutes ( $\lambda_{\text{ex}} = 362 \text{ nm}$ ).

### 3.6.6 Competitive experiments over other metal ions

The selectivity toward  $\text{Au}^{3+}$  ion was further ascertained by the competitive experiment employed by the addition of 50 equiv of competing metal ions to the Et-DHP-AC(3)• $\text{Au}^{3+}$  (1:10 equiv) mixtures. The interference can be determined in bar diagram from plotting of  $(I_{\text{Au}} - I_0)/(I - I_0)$  value against the types of metal ions. Where  $I_0$  = Maximum fluorescence intensity of Et-DHP-AC(3) without any metal ions,  $I_{\text{Au}}$  = Maximum fluorescence intensity of Et-DHP-AC(3) with  $\text{Au}^{3+}$ ,  $I$  = Maximum fluorescence intensity of Et-DHP-AC(3) with  $\text{Au}^{3+}$  and other metal ions. Therefore,

without the interference from other metal ions, the value at y axis should equal to 1. The fluorescence quenching efficiency of  $\text{Au}^{3+}$  ion was slightly inhibited in the presence of  $\text{Bi}^{3+}$  but in case of  $\text{Li}^+$  and  $\text{Mn}^{2+}$  (Figure 3.18). It might be resulted from  $\text{Bi}^{3+}$ ,  $\text{Li}^+$ , and  $\text{Mn}^{2+}$  disturb the reaction by expelling fluorophore away from  $\text{Au}^{3+}$  ions.

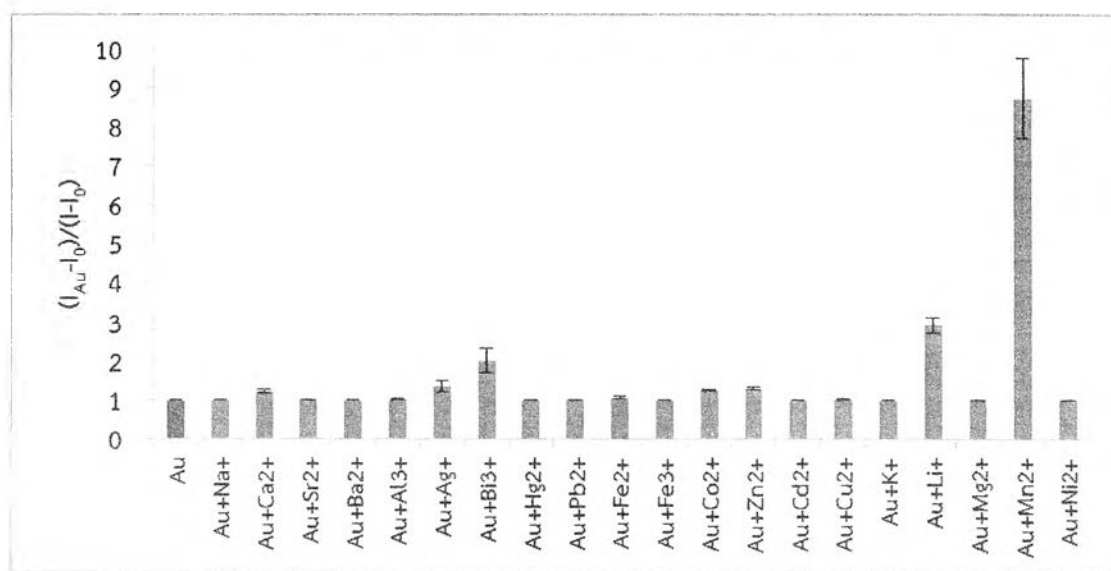


**Figure 3.18** Competitive experiments in the Et-DHP-AC(3) with  $\text{Au}^{3+}$  system with interfering metal ions ( $\text{Mn}^{n+}$ ).  $[\text{Et-DHP-AC}(3)] = 10 \mu\text{M}$ ,  $[\text{Au}^{3+}] = 100 \mu\text{M}$ , and  $[\text{M}^{n+}] = 500 \mu\text{M}$  in milliQ water.

### 3.6.7 Job's method

Job's method was applied to determine the stoichiometry of Et-DHP-AC(3) and  $\text{Au}^{3+}$ . To implement experimentally Job's method, a series of solutions with fixed total concentration of Et-DHP-AC(3) and  $\text{Au}^{3+}$  were prepared, but in which their mole fractions were varied. This proportional complex formation is plotted against the mole fractions of these two components, demonstrating the maximum corresponding to the stoichiometry of two species. A Job's plot, which exhibits a maximum at 0.5 mol fraction, indicates that the structural change stoichiometrically and most efficiently occurred at the mixture ratio of 1:1 (Figure 3.19).

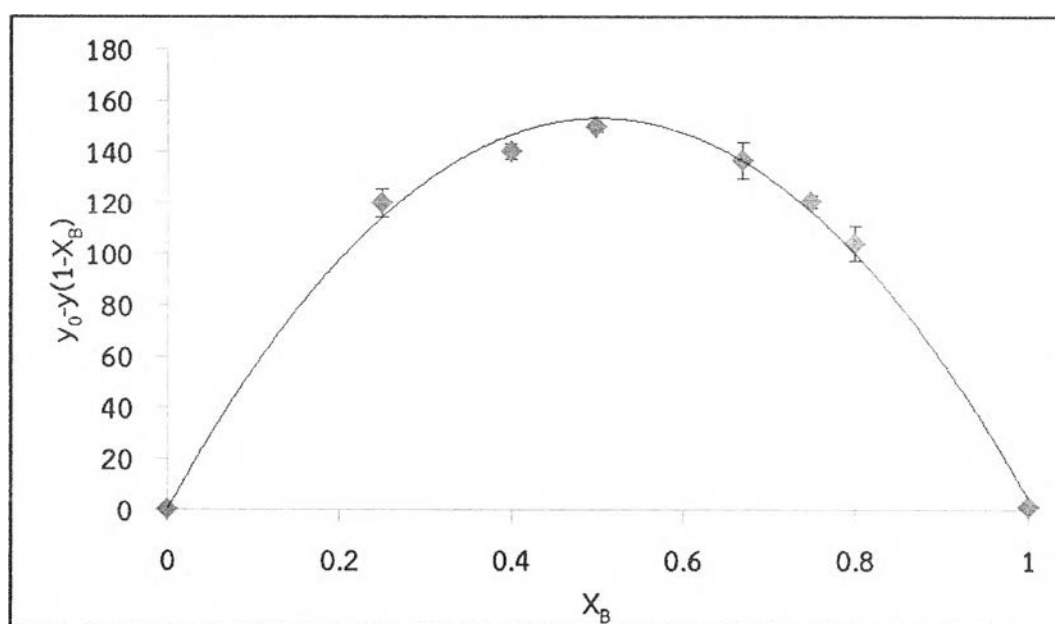


Figure 3.19 Job's plot of Et-DHP-AC(3) in 1:1 stoichiometry with  $\text{Au}^{3+}$ .

### 3.6.8 Metal detection of Et-DHP-AC(3)

#### i) Study of solvent effect on fluorescence enhancement

Et-DHP-AC(3) includes azacrown ether ring as water soluble moiety and available receptor in particular with alkaline and alkaline earth metal. Thus, in order to see the solvent effect on azacrown ring, the study in solvent mixture between aqueous milliQ water and organic solvent; acetonitrile and THF was undertaken with various mixed ratio of Et-DHP-AC(3) 10  $\mu\text{M}$  and metal complex ion 1,000  $\mu\text{M}$  (Figure 3.20). In the investigation conditions of acetonitrile and milliQ water

85:15, the fluorescence intensity of Et-DHP-AC(3) was increased by  $K^+$  (42%),  $Sr^{2+}$  (72%), and  $Ba^{2+}$  (74%) (Table 3.2).

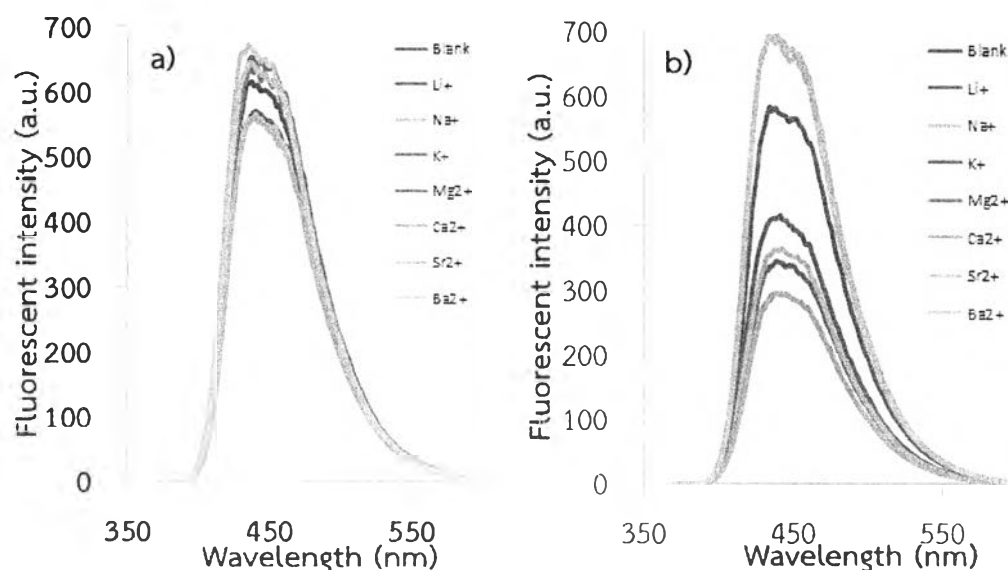


**Figure 3.20** Fluorescence enhancing profile of Et-DHP-AC(3) (10  $\mu$ M) after addition of each metal ion (1,000  $\mu$ M). a) THF and milliQ water 85:15, b) acetonitrile and milliQ water 85:15.

As a result from **Table 3.2**, the organic solvent helped to increase the percent enhancement, hence THF and acetonitrile (ACN) was selected for studying fluorescence enhancement. At the ratio of THF and MQ 50:50, Et-DHP-AC(1-3) was the same enhancement as at the ratio of ACN and MQ 50:50. Considerably, the ratio of ACN and MQ of 85:15 provided the highest enhancement whereas THF and MQ of 85:15 gave the lowest enhancement. Thereby, the fluorescence enhancement was studied in mixed solvent of ACN and MQ.

According to the results of enhancement experiment, both  $Ba^{2+}$  and  $Sr^{2+}$  ion showed higher enhancement in condition of ACN and MQ of 70:30. The highest enhancement for  $K^+$  was the one under the condition of ACN and MQ of 80:20 (**Table 3.3**). Interestingly, in case of  $Ba^{2+}$  in ACN and MQ of 70:30, is the highest enhancement among others was exhibited. So  $Ba^{2+}$  as metal ion was selected to further study other factors in these mixed solvents (70:30).

**Table 3.2** %Fluorescence enhancement of Et-DHP-AC(3)  $K^+$ ,  $Sr^{2+}$ , and  $Ba^{2+}$  in milliQ water (MQ) and organic solvent.

ACN: MQ (ratio)	Blank ( $I_0$ )	$K^+$		$Sr^{2+}$		$Ba^{2+}$	
		$I_{max}$	%Enh	$I_{max}$	%Enh	$I_{max}$	%Enh
50:50	434	478	10	590	36	675	56
60:40	413	474	15	572	38	625	51
70:30	348	432	24	655	88	700	101
80:20	338	522	54	636	88	664	96
85:15	400	569	42	690	72	695	74

MQ = milliQ water and ACN = acetonitrile

$$*\%Enhancement (\%Enh) = [(I_{max}-I_0)/I_0] \times 100$$

**Table 3.3** %Fluorescence enhancement of Et-DHP-AC(3)  $K^+$ ,  $Sr^{2+}$ , and  $Ba^{2+}$  at various ratio of MQ and ACN.

Condition	Blank ( $I_0$ )	$K^+$		$Sr^{2+}$		$Ba^{2+}$	
		$I_{max}$	%Enh*	$I_{max}$	%Enh*	$I_{max}$	%Enh*
MQ	551	577	4.7	575	4	577	5
ACN: MQ (85:15)	400	569	42	690	72	695	74
ACN: MQ (50:50)	434	478	10	590	35	675	56
THF: MQ (85:15)	636	640	1	650	2	645	1
THF: MQ (50:50)	290	334	15	420	45	485	67

## ii) Metal ion sensing with Et-DHP-AC(3)·Ba<sup>2+</sup>

Et-DHP-AC(3)·Ba<sup>2+</sup> as a new complex sensor is supposed to possess the allosteric property. Based on the hypothesis of this experiment, Ba<sup>2+</sup> ion may adjust the energy gap HOMO or LUMO and affect to the selectivity and the sensitivity of Et-DHP-AC(3)·Ba<sup>2+</sup>. Therefore, The fluorescence responses of Et-DHP-AC(3)·Ba<sup>2+</sup> (10 μM:1,000 μM) towards 20 metal ions (Na<sup>+</sup>, Ca<sup>2+</sup>, Al<sup>3+</sup>, Ag<sup>+</sup>, Cr<sup>3+</sup>, Hg<sup>2+</sup>, Pb<sup>2+</sup>, Fe<sup>2+</sup>, Fe<sup>3+</sup>, Co<sup>2+</sup>, Zn<sup>2+</sup>, Cd<sup>2+</sup>, Cu<sup>2+</sup>, K<sup>+</sup>, Li<sup>+</sup>, Mg<sup>2+</sup>, Mn<sup>2+</sup>, Ni<sup>2+</sup>, Sn<sup>2+</sup>, and Au<sup>3+</sup>) were carried out. However, Et-DHP-AC(3)·Ba<sup>2+</sup> was not selective to any metal ion (Figure 3.15). Even though, Sr<sup>2+</sup> and K<sup>+</sup> ions are less enhancing than Ba<sup>2+</sup> ion, they were also tried for metal ion sensing whether they may generate the allosteric mode with Et-DHP-AC(3). Unfortunately, in this mixed solvent system, both Sr<sup>2+</sup> and K<sup>+</sup> ion were not selective and sensitive to any other metal ions (Figure 3.16 and 3.17). Surprisingly, Au<sup>3+</sup> ion did not quench Et-DHP-AC(3) as it did in MQ. We attempted to investigate Et-DHP-AC(3) without Ba<sup>2+</sup> to sense with Au<sup>3+</sup> in ACN and MQ of 70:30. The result from Figure 3.23 exhibited that the more organic solvent was increased, the more quenching process of Au<sup>3+</sup> was inhibited.

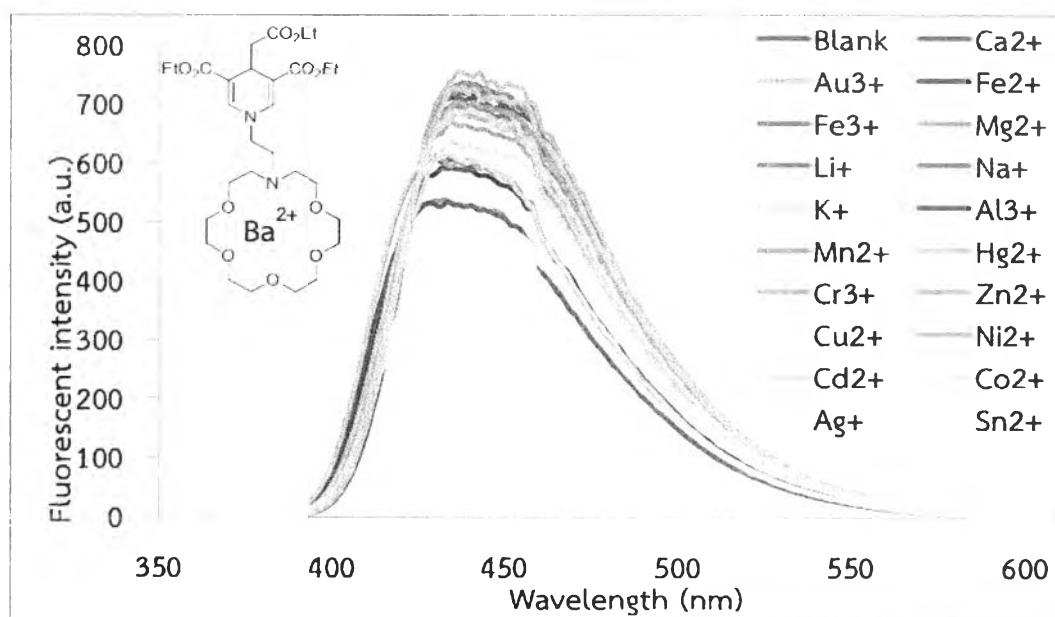


**Figure 3.21** Fluorescence intensity of Et-DHP-AC(3)·Ba<sup>2+</sup> (10 μM:1,000 μM), 10 minutes after addition of each metal ion (100 μM) in acetonitrile and milliQ water (70:30), λ<sub>ex</sub> = 362 nm.



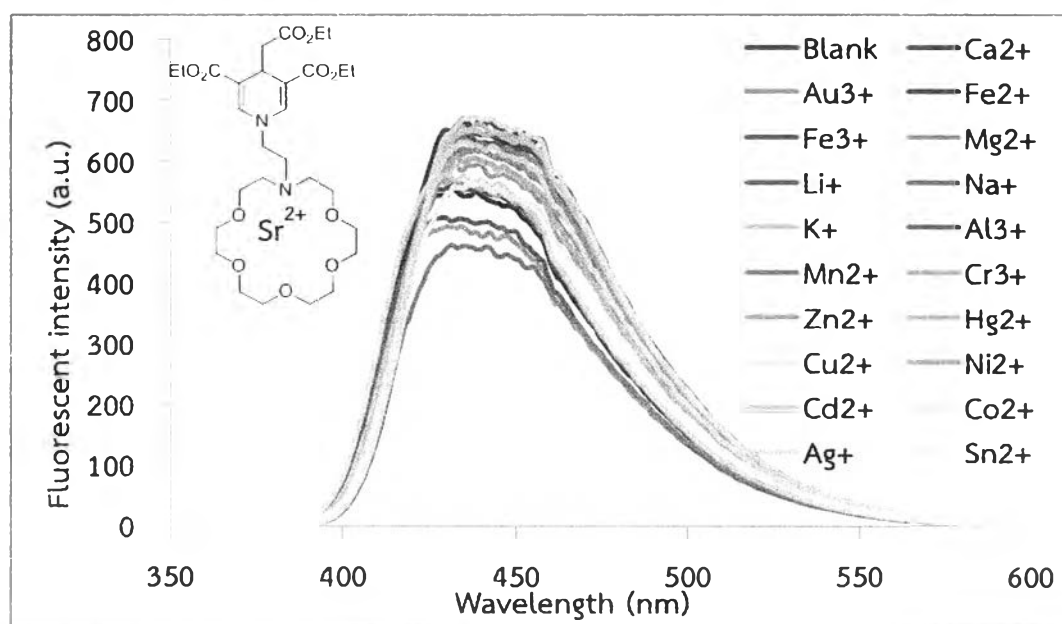


**Figure 3.22** Fluorescence intensity of Et-DHP-AC(3)·Sr<sup>2+</sup> (10 μM:1,000 μM), 10 minutes after addition of each metal ion (100 μM) in acetonitrile and milliQ water (70:30),  $\lambda_{\text{ex}}$  = 362 nm.

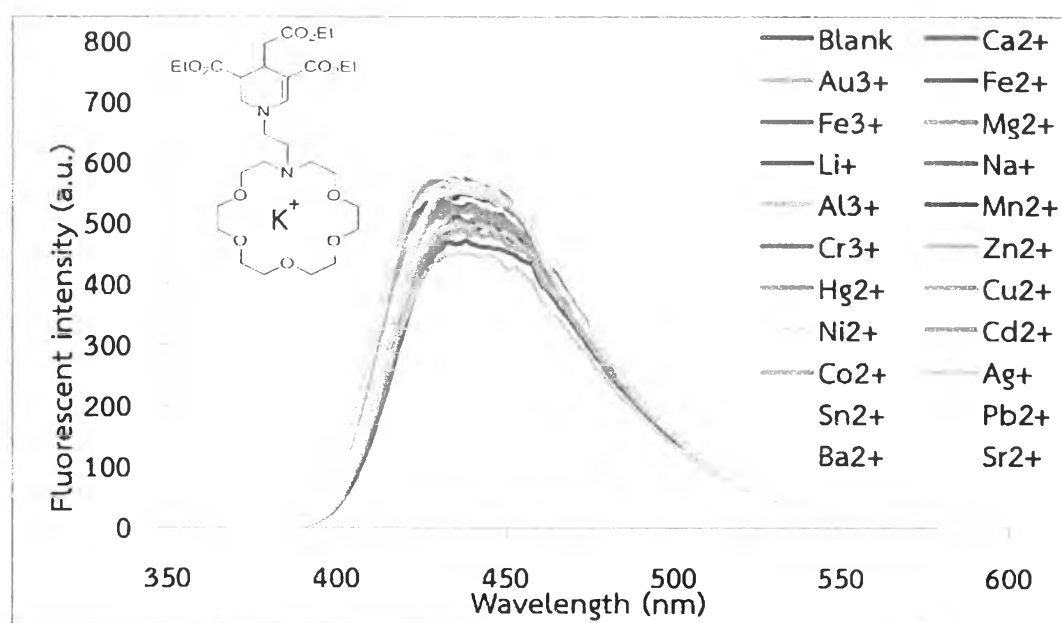


**Figure 3.23** Fluorescence intensity of Et-DHP-AC(3)·K<sup>+</sup> (10 μM:1,000 μM), 10 minutes after addition of each metal ion (100 μM) in acetonitrile and milliQ water (70:30),  $\lambda_{\text{ex}}$  = 362 nm.

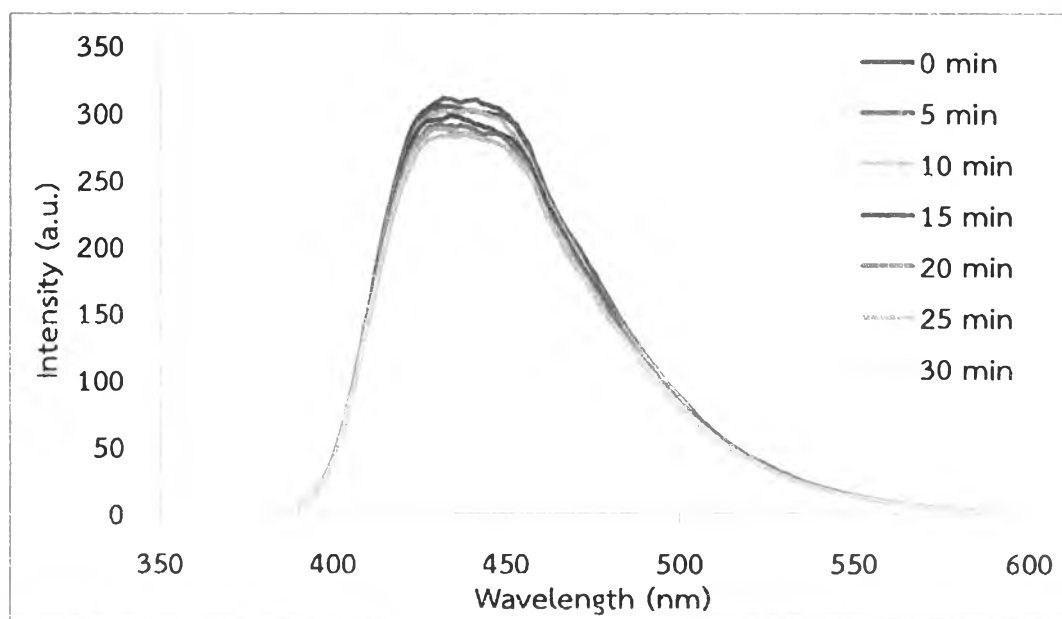


**Figure 3.24** Fluorescence intensity of Et-DHP-AC(3) with Au<sup>3+</sup> in acetonitrile and milliQ water (70:30).

iii) Comparison of enhancing intensity of Et-DHP-OH, Et-DHP-NEt<sub>2</sub>, and Et-DHP-AC(3)

To study process of enhancing intensity of Et-DHP-AC(3) with K<sup>+</sup>, Sr<sup>2+</sup>, and Ba<sup>2+</sup> as metal complex ion, the comparison with Et-DHP-OH or Et-DHP-NEt<sub>2</sub> in the mixture solvent between acetonitrile and milliQ water of 70:30 was needed. Et-DHP-OH and Et-DHP-NEt<sub>2</sub> did not enhance with K<sup>+</sup>, Sr<sup>2+</sup>, Ba<sup>2+</sup> but Et-DHP-AC(3) occurred fluorescent enhancement because the effect of azacrown ether induced and formed complex with metal ion. The complexation affected to reduce the energy for using rotation and vibration thus the fluorescence emission was increase.

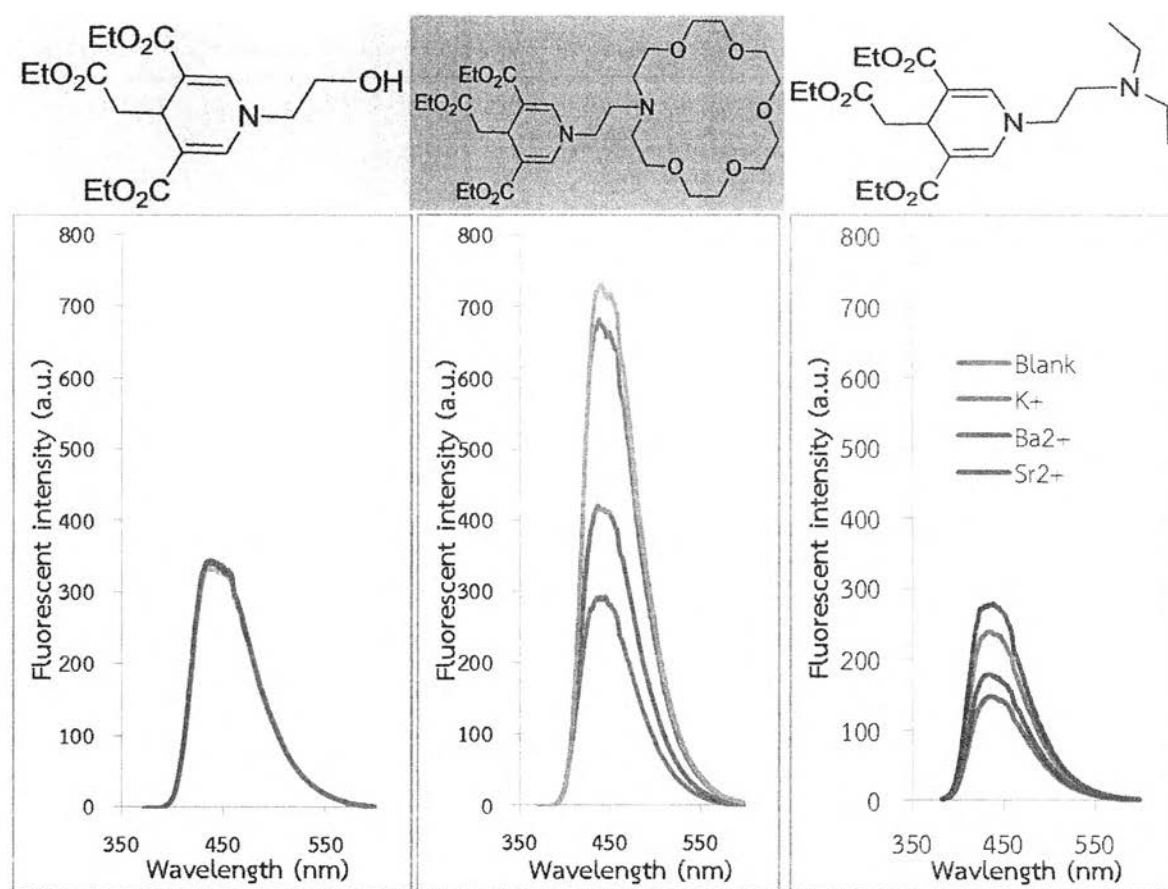
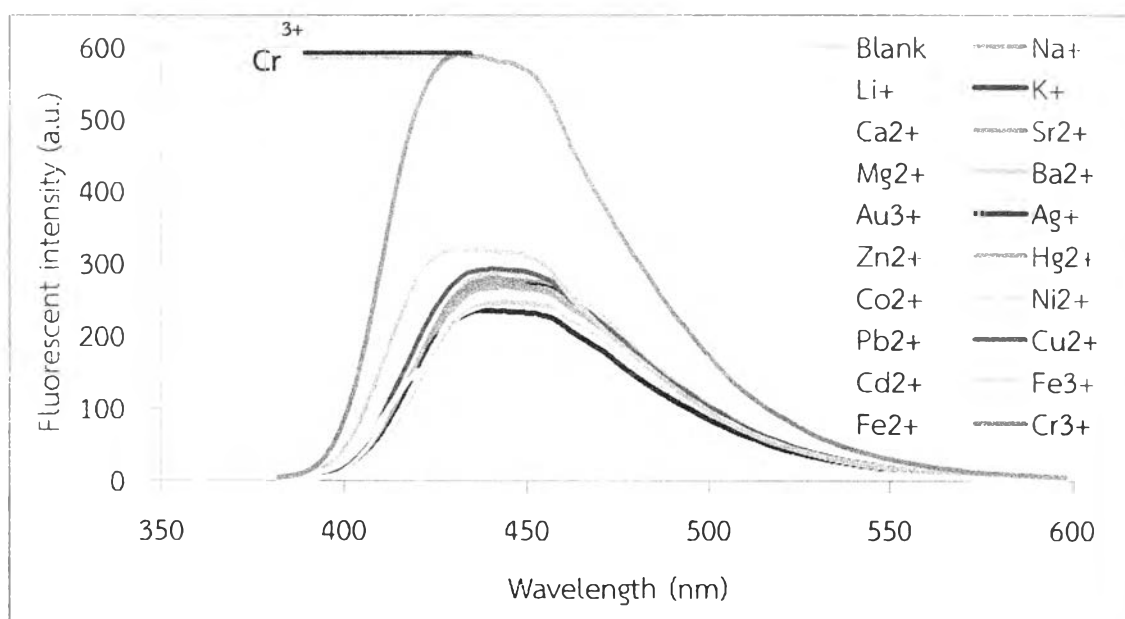


Figure 3.25 Fluorescence intensity of Et-DHP-OH, Et-DHP-NEt<sub>2</sub>, and Et-DHP-AC(3) (10 μM), 10 minutes after addition of K<sup>+</sup>, Sr<sup>2+</sup>, and Ba<sup>2+</sup> (1,000 μM) in acetonitrile and milliQ water (70:30).

### 3.7 Metal ion sensor of Et-DHP-AC(2)

#### 3.7.1 Selectivity study

The fluorescence responses of Et-DHP-AC(2) (10  $\mu\text{M}$ ) in THF and milliQ water (v/v 1:1) towards 19 metal ions (100 equiv) ( $\text{Li}^+$ ,  $\text{Na}^+$ ,  $\text{K}^+$ ,  $\text{Mg}^{2+}$ ,  $\text{Ca}^{2+}$ ,  $\text{Sr}^{2+}$ ,  $\text{Ba}^{2+}$ ,  $\text{Au}^{3+}$ ,  $\text{Ag}^+$ ,  $\text{Zn}^{2+}$ ,  $\text{Hg}^{2+}$ ,  $\text{Co}^{2+}$ ,  $\text{Ni}^{2+}$ ,  $\text{Pb}^{2+}$ ,  $\text{Cu}^{2+}$ ,  $\text{Cr}^{3+}$ ,  $\text{Cd}^{2+}$ ,  $\text{Fe}^{2+}$ ,  $\text{Fe}^{3+}$ ) were achieved **Figure 3.26**. Et-DHP-AC(2) was found to have the best selectivity with chromium(III) by enhancing mechanism. Though the response towards  $\text{Cr}^{3+}$  was still the highest one, the addition of 10 equiv of metal ions;  $\text{Fe}^{2+}$ ,  $\text{Fe}^{3+}$ , and  $\text{Au}^{3+}$  also happened to enhance the fluorescent intensity of Et-DHP-AC(2) (**Figure 3.27**). For  $\text{Au}^{3+}$  and  $\text{Fe}^{3+}$  have possibly the same ionic charge as chromium(III) ion, they also suitably bind with azacrown ring. In case of  $\text{Fe}^{2+}$ , it might be oxidized into  $\text{Fe}^{3+}$  due to instability during the excitation with UV through the reaction with  $\text{O}_2$  in air.



**Figure 3.26** Fluorescence enhancing profile of Et-DHP-AC(2) (10  $\mu\text{M}$ ) after addition of each metal ion (1000  $\mu\text{M}$ ) in THF and milliQ water (v/v = 1:1) ( $\lambda_{\text{ex}} = 369 \text{ nm}$ ).

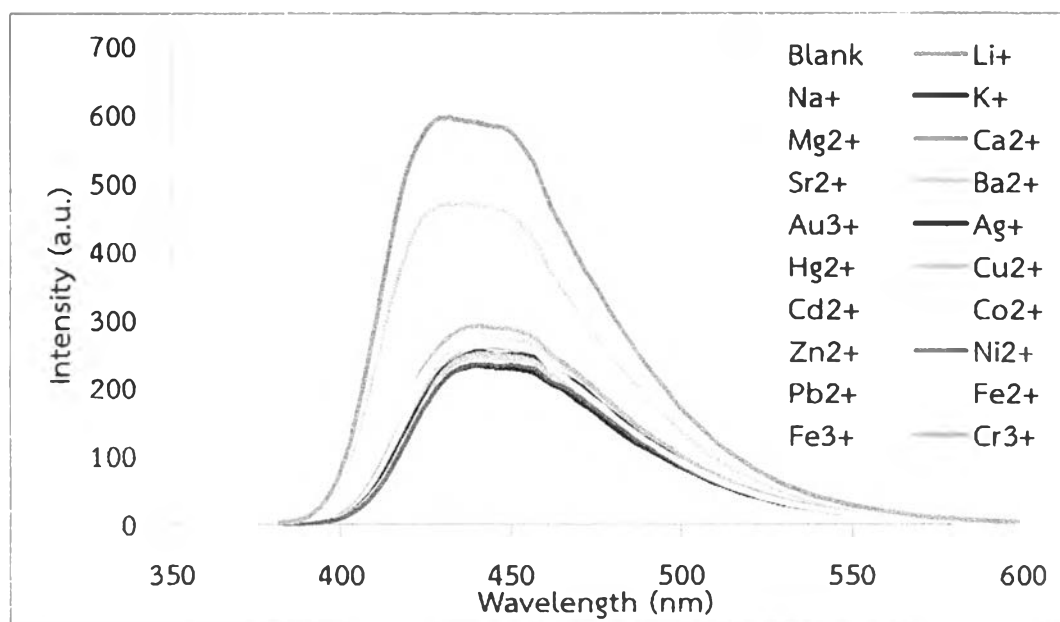


**Figure 3.27** Fluorescence enhancing profile of Et-DHP-AC(2) (10  $\mu\text{M}$ ) after addition of each metal ion (100  $\mu\text{M}$ ) in THF and milliQ water (v/v = 1:1) ( $\lambda_{\text{ex}}$  = 369 nm).

### 3.7.2 Fluorescence response

The fluorescence intensity of Et-DHP-AC(2) (10  $\mu\text{M}$ ) in THF and milliQ water (v/v = 1:1) toward metal ions was performed. Upon addition of amount of chromium(III) ion from 0 to 10 equiv (100  $\mu\text{M}$ ), the enhancing in fluorescence emission was observed at concentration as high as 10 equiv (Figure 3.28). The chromium(III) ion at 1-4 equiv has not enhanced the fluorescence intensity whereas 5 equiv slightly started to enhance. Since, Stern-Volmer plot  $I/I_0$  against amount of  $\text{Cr}^{3+}$  showed nonlinear curve (s-curve), the method reported by Bhalla was then needed for the determination of the lowest detectable concentration (50  $\mu\text{M}$ ) (Figure 3.29).

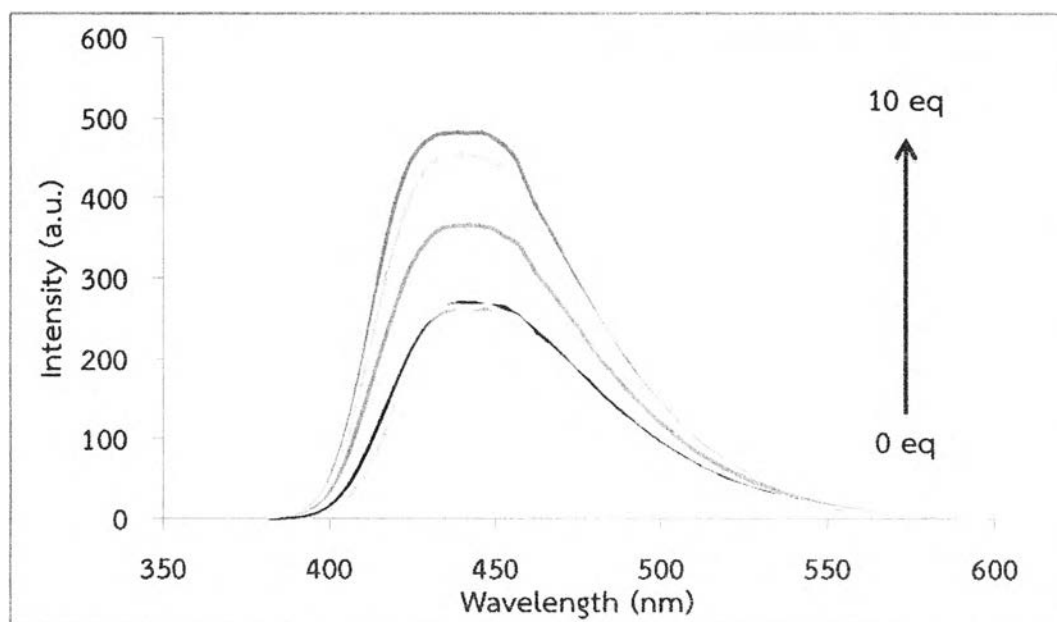


Figure 3.28 Fluorescence change of Et-DHP-AC(2) (10 μM) with the addition of Cr<sup>3+</sup> (0 to 10 equiv) in THF and milliQ water (v/v = 1:1) ( $\lambda_{\text{ex}} = 369 \text{ nm}$ ).

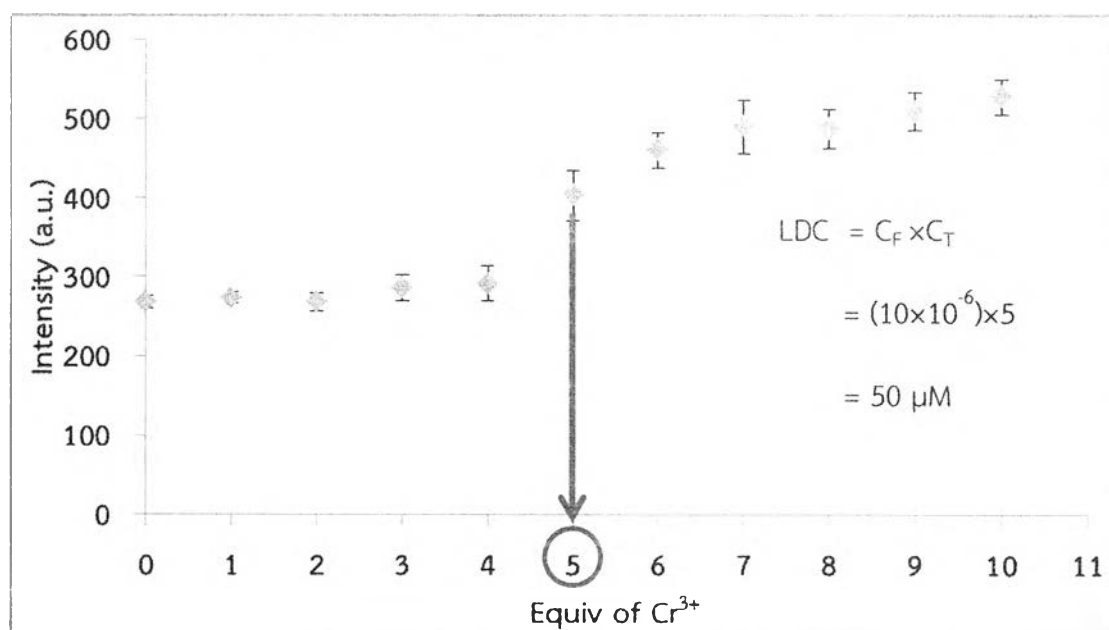
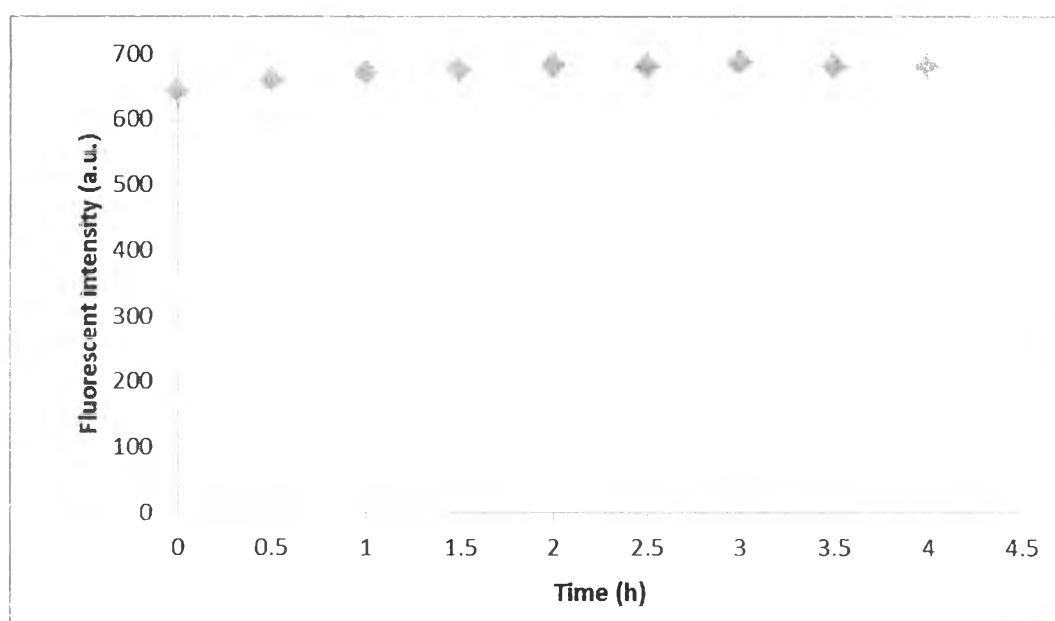


Figure 3.29 Fluorescence change of Et-DHP-AC(2) (10 μM) with the addition of Cr<sup>3+</sup> (0 to 10 equiv) in THF and milliQ water (v/v = 1:1) ( $\lambda_{\text{ex}} = 369 \text{ nm}$ ).

### 3.7.3 Stability study of Et-DHP-AC(2) after enhancing monitoring

In addition, the kinetic response of Et-DHP-AC(2) to chromium(III) ion was investigated by monitoring the fluorescence intensity of Et-DHP-AC(2) solution after incubation with chromium(III) ion for 4 h. As shown in **Figure 3.30** the fluorescence intensity of Et-DHP-AC(2) was not changed at all even after 4 h, displaying that the fluorescence enhancing rate was very fast and the complex was stable in a long period of time (at least 4 h).



**Figure 3.30** Effect of time on the fluorescence enhancing reaction between Et-DHP-AC(2) (10  $\mu\text{M}$ ) and chromium(III) (1,000  $\mu\text{M}$ ).

### 3.7.4 Competitive experiments over other metal ions

The selectivity toward  $\text{Cr}^{3+}$  ion was further ascertained by the competitive experiment employed by the addition of 100 equiv of competing metal ions to the Et-DHP-AC(2): $\text{Cr}^{3+}$  (1:10 equiv) mixtures. The interference can be determined in bar diagram from plotting of  $(I_0 - I_m)/(I_0 - I_{\text{Cr}})$  value against the types of metal ion. Where  $I_0$  = Maximum fluorescence intensity of Et-DHP-AC(2) without any metal ions,  $I_{\text{Cr}}$  = Maximum fluorescence intensity of Et-DHP-AC(2) with  $\text{Cr}^{3+}$ ,  $I$  = Maximum fluorescence intensity of Et-DHP-AC(2) with  $\text{Cr}^{3+}$  and other metal ions. Therefore, without the interference from other metal ions, the value at y axis is equal to 1. The fluorescence enhancing efficiency of  $\text{Cr}^{3+}$  ion was interfered by  $\text{Au}^{3+}$ ,  $\text{Fe}^{2+}$ ,  $\text{Fe}^{3+}$ ,  $\text{Cu}^{2+}$ ,  $\text{Ag}^+$ ,  $\text{Zn}^{2+}$ , and  $\text{Pb}^{2+}$ . These interfering metal ions were suspected that the high concentration of these metal ions (1000 equiv) might disturb the binding between fluorophore and  $\text{Cr}^{3+}$  (100 equiv). Additionally,  $\text{Au}^{3+}$  has potentially quenched the Et-DHP-AC(2) through the oxidation of pyridine ring into pyridinium, it therefore affected to decrease the fluorescent intensity (Figure 3.31).  $\text{Fe}^{2+}$  and  $\text{Fe}^{3+}$ , In the case of competitive absorption can be considered.

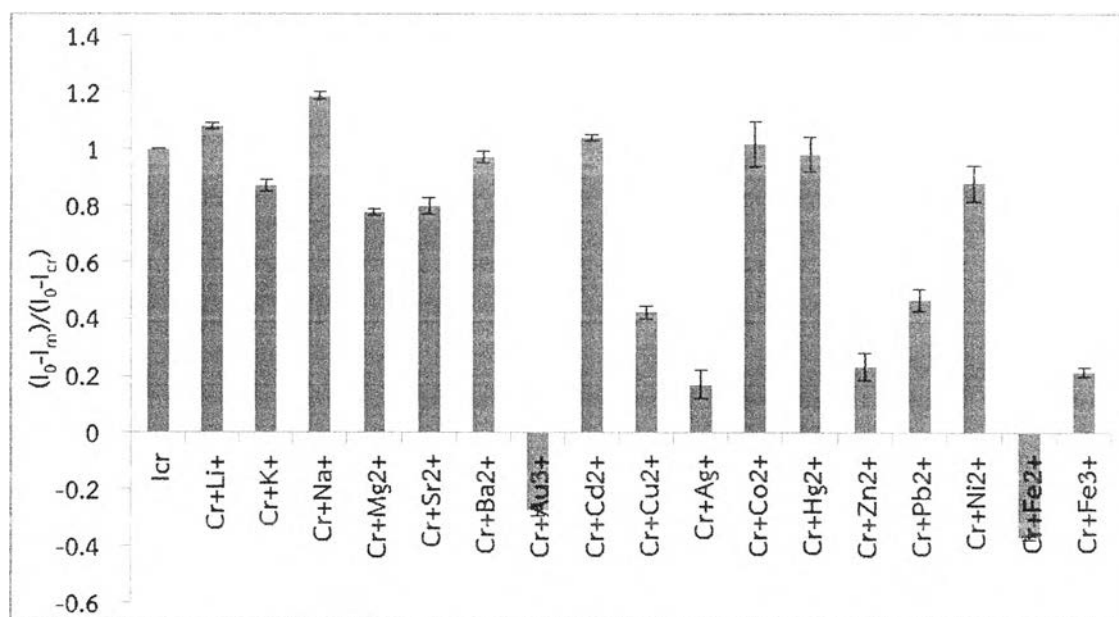


**Figure 3.31** Competitive experiments in the Et-DHP-AC(2) system with interfering metal ions.  $[\text{Et-DHP-AC}(2)] = 10 \mu\text{M}$ ,  $[\text{Cr}^{3+}] = 100 \mu\text{M}$ , and  $[\text{M}^{n+}] = 1000 \mu\text{M}$  in THF and milliQ water ( $v/v = 1:1$ ) ( $\lambda_{\text{ex}} = 369 \text{ nm}$ ).



### 3.7.5 Job's method

Job's method of continuous variation was of concentration applied to determine the stoichiometry of Et-DHP-AC(2) and  $\text{Cr}^{3+}$ . To implement Job's method experimentally, a series of solutions containing a fixed total number of moles of Et-DHP-AC(2) and  $\text{Cr}^{3+}$  were prepared, but in which their mole fractions were varied. This proportional complex formation is plotted against the mole fractions of these two components, demonstrating the maximum corresponding to the stoichiometry of two species. A Job's plot, which exhibits a maximum at 0.25 mol fraction, indicates that the structural change stoichiometrically and most efficiently occurred at the mixture ratio of 3:1 (Figure 3.32).

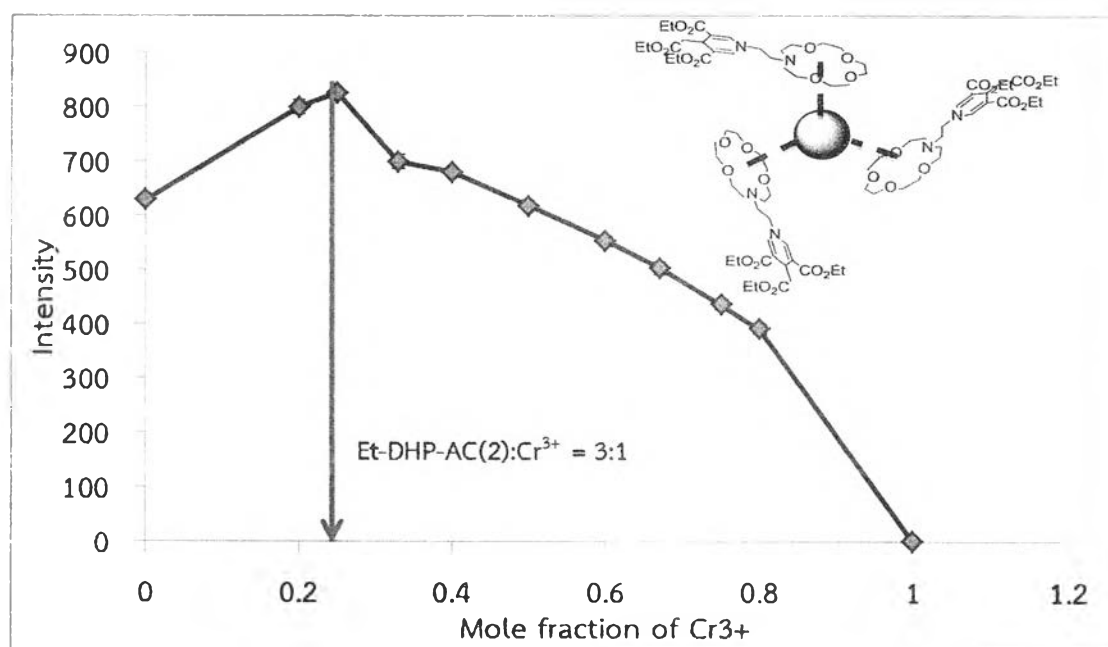


Figure 3.32 Job's plot of Et-DHP-AC(2) in 3:1 stoichiometry with  $\text{Cr}^{3+}$ .

### 3.8 Nitroaromatic explosive sensor

There are many analysis methods which were used for explosive sensing such as LC-MS [35, 36], GC-MS [37], HPLC [38, 39], ion mobility spectrometry [40, 41], and proton transfer reaction-mass spectrometry (PTR-MS) [42], but their disadvantages are high cost, complicated using, and expensive instruments. The fluorescence detection therefore becomes one of the most promising methods for explosive sensing because of several advantages; high sensitivity, selectivity, specificity, and real-time monitoring with short response time. Due to the powerful explosiveness and deleterious pollution of nitroaromatic compounds, they have become a worldwide concerns of public security, terrorist activity, and environmental problem [43] especially, both 2,4,6-trinitrotoluene (TNT) and 2,4,6-trinitrophenol (TNP) or picric acid. TNP is a superior explosive than TNT [44] and also causes severe irritation, skin allergy, dizziness, nausea, damage of liver and kidney [45, 46]. So Et-DHP-AC(3) was demonstrated in nitroaromatic sensing study. Nine types of nitroaromatic compounds were used in this study; 2,4,6-trinitrophenol (TNP), 2,4,6-trinitrotoluene (TNT), 2,4-dinitrotoluene (DNT), 2-chlorobenzoic acid (2CBA), 4-nitrobenzene (4NT), 4-nitrobenzoic acid (4NBA), 2,4-dinitrophenol (DNP), 3-nitrophenol (3NP), and 4-nitrophenol (4NP) (Figure 3.33). Two types of nitroaromatic compounds, TNP and DNP, selectively quenched Et-DHP-AC(3) (Figure 3.34-3.35).

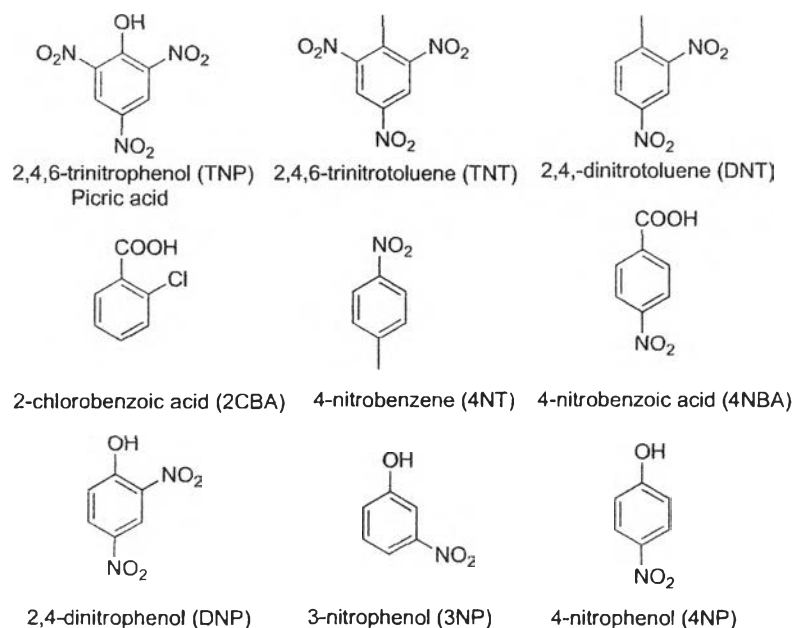
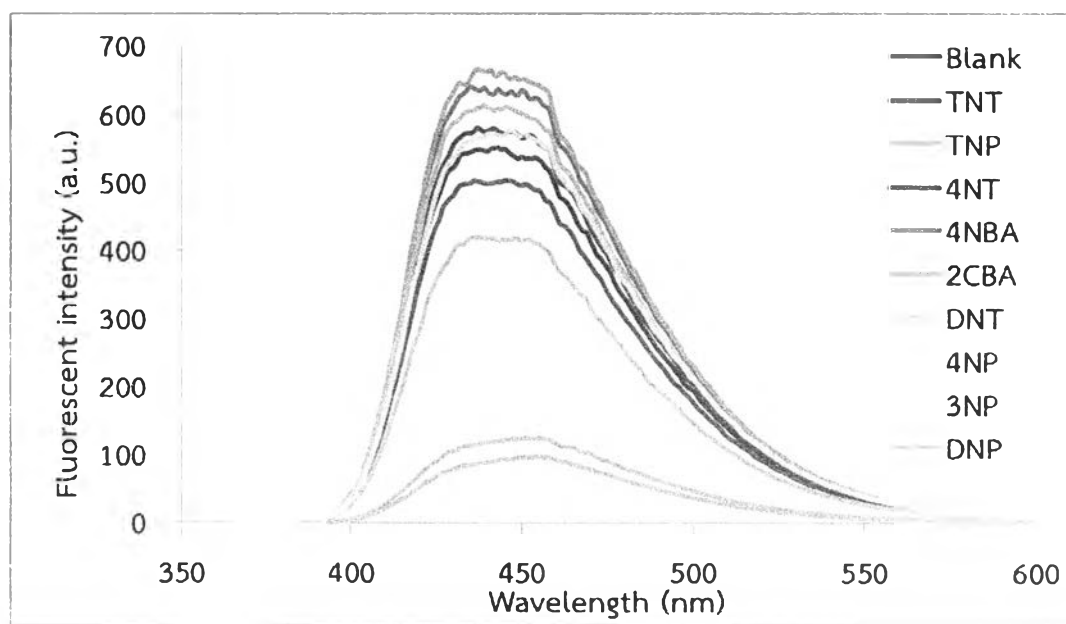
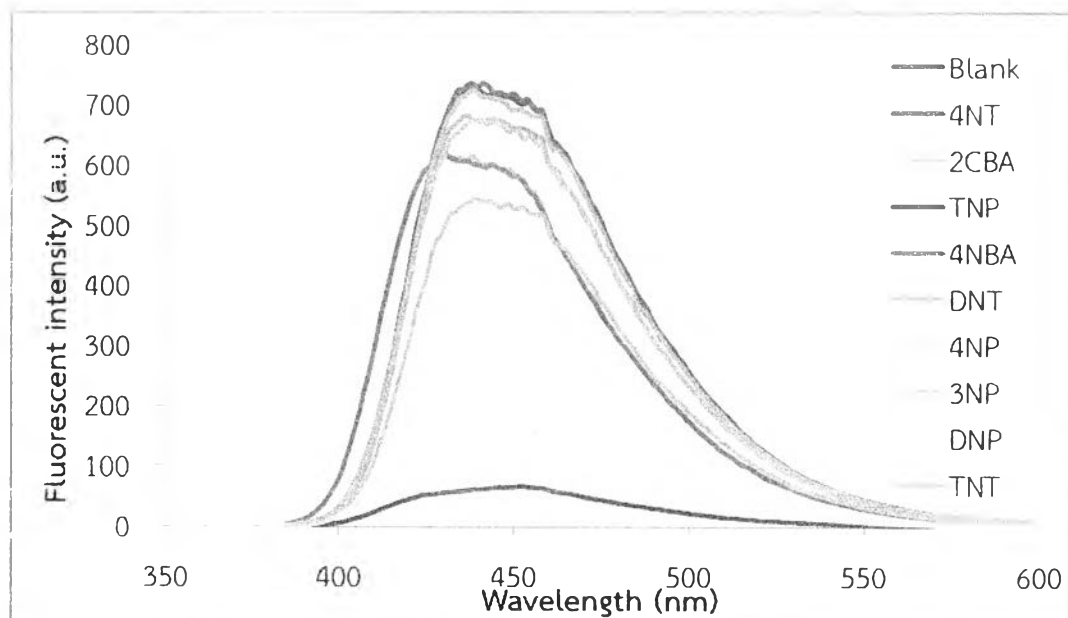


Figure 3.33 All of nitroaromatic explosive compounds used in the study.



**Figure 3.34** Fluorescence quenching profile of Et-DHP-AC(3) (10  $\mu\text{M}$ ), after addition of each nitroaromatic compound (100  $\mu\text{M}$ ) in milliQ ( $\lambda_{\text{ex}} = 362 \text{ nm}$ ).



**Figure 3.35** Fluorescence quenching profile of Et-DHP-AC(3) (10  $\mu\text{M}$ ) with  $\text{Ba}^{2+}$  (1,000  $\mu\text{M}$ ) after addition of each nitroaromatic compound (100  $\mu\text{M}$ ) in mixture solvent between acetonitrile and milliQ water (70:30) ( $\lambda_{\text{ex}} = 362 \text{ nm}$ ).

In the case of Et-DHP-AC(3)· $\text{Ba}^{2+}$  complex, The decrease of fluorescence signal was proportional to TNP and DNP concentration. The fluorescence quenching is

probably due to the competitive absorption and the energy transfer from the excited state of Et-DHP-AC(3) to the ground state of TNP via the spectra overlap of the absorption of TNP and emission of the Et-DHP-AC(3) in the wavelength region of 400-480 nm. Hence, both Et-DHP-AC(3) and Et-DHP-AC(3)·Ba<sup>2+</sup> complex were not suitable for detecting TNP and DNP in real sample.